6-3-2015

Butterfly pitch-angle distribution of relativistic electrons in the outer radiation belt: Evidence of nonadiabatic scattering

Nikolai O. Artemyev
University of Iowa

O. V. Agapitov
University of California - Berkeley

F. S. Mozer
University of California - Berkeley

Harlan E. Spence
University of New Hampshire, harlan.spence@unh.edu

Recommended Citation

Artemyev, A. V., O. V. Agapitov, F. S. Mozer, and H. Spence (2015), Butterfly pitch angle distribution of relativistic electrons in the outer radiation belt: Evidence of nonadiabatic scattering, J. Geophys. Res. Space Physics, 120, 4279–4297, doi:10.1002/2014JA020865.

AGU PUBLICATIONS

JGR

Journal of Geophysical Research: Space Physics

RESEARCH ARTICLE
10.1002/2014JA020865

Special Section:
New perspectives on Earth's radiation belt regions from the prime mission of the Van Allen Probes

Butterfly pitch angle distribution of relativistic electrons in the outer radiation belt: Evidence of nonadiabatic scattering

A. V. Artemyev[1,2], O. V. Agapitov[1,3], F. S. Mozer[1], and H. Spence[4]

[1]Space Science Laboratory, University of California, Berkeley, California, USA, [2]Space Research Institute, RAS, Moscow, Russia, [3]Astronomy and Space Physics Department, Physical Faculty, Taras Shevchenko National University of Kiev, Kiev, Ukraine, [4]Department of Physics, University of New Hampshire, Durham, New Hampshire, USA

Abstract In this paper we investigate the scattering of relativistic electrons in the nightside outer radiation belt (around the geostationary orbit). We consider the particular case of low geomagnetic activity ($|D_{st}| < 20$ nT), quiet conditions in the solar wind, and absence of whistler wave emissions. For such conditions we find several events of Van Allen probe observations of butterfly pitch angle distributions of relativistic electrons (energies about 1–3 MeV). Many previous publications have described such pitch angle distributions over a wide energy range as due to the combined effect of outward radial diffusion and magnetopause shadowing. In this paper we discuss another mechanism that produces butterfly distributions over a limited range of electron energies. We suggest that such distributions can be shaped due to relativistic electron scattering in the equatorial plane of magnetic field lines that are locally deformed by currents of hot ions injected into the inner magnetosphere. Analytical estimates, test particle simulations, and observations of the *AE* index support this scenario. We conclude that even in the rather quiet magnetosphere, small scale (magnetic local time (MLT)-localized) injection of hot ions from the magnetotail can likely influence the relativistic electron scattering. Thus, observations of butterfly pitch angle distributions can serve as an indicator of magnetic field deformations in the nightside inner magnetosphere. We briefly discuss possible theoretical approaches and problems for modeling such nonadiabatic electron scattering.

Key Points:
- Observations of butterfly pitch angle distributions of MeV electrons
- Nonadiabatic scattering in disturbed dipole magnetic fields
- Role of small-scale injections in scattering of MeV electrons

Supporting Information:
- Text S1
- Figure S1
- Figure S2
- Figure S3
- Figure S4
- Figure S5
- Figure S6
- Figure S7

Correspondence to:
A. V. Artemyev,
ante0226@gmail.com

Citation:
Artemyev, A. V., O. V. Agapitov, F. S. Mozer, and H. Spence (2015), Butterfly pitch angle distribution of relativistic electrons in the outer radiation belt: Evidence of nonadiabatic scattering, *J. Geophys. Res. Space Physics*, *120*, 4279–4297, doi:10.1002/2014JA020865.

Received 20 NOV 2014
Accepted 27 APR 2015
Accepted article online 4 MAY 2015
Published online 3 JUN 2015

1. Introduction

The motion of charged particles in the Earth's inner magnetosphere is controlled by the strong dipole magnetic field. Such motions are called adiabatic due to the conservation of the three adiabatic invariants corresponding to particle gyrorotation (the first adiabatic invariant—magnetic moment), bounce oscillations (the second adiabatic invariant), and azimuthal drift around the planet (third adiabatic invariant) [see, e.g., *Roederer*, 1970; *Shabansky*, 1971; *Ukhorskiy and Sitnov*, 2013, and references therein]. The nonconservation of these invariants has been the subject of detailed investigations throughout the history of radiation belt physics.

There are two main mechanisms responsible for nonadiabatic effects: various peculiarities of the magnetic field configuration and wave-particle resonance interactions. In the first case we deal with the violation of the adiabatic approximation when the scale size of the magnetic field inhomogeneity becomes comparable to the spatial scale (say Larmor radius) of charged particle motion. The second case produces violation of the adiabatic approximation due to fast (comparable with the time scale of charged particle gyrorotation) variations of wave electromagnetic fields. Thus, shaping of charged particle pitch angle distributions is controlled by transport (and/or injection) processes in a deformed dipole magnetic field (these mechanisms seem to be more important for ions, see *Chen et al.* [1998], *Anderson and Takahashi* [2000], and *Ebihara et al.* [2011]) and by the wave-particle resonant interactions (seem to be more important for electrons, see, e.g., *Åsnes et al.* [2005]).

One of the beautiful manifestations of nonadiabatic effects of charged particle motion in the inner magnetosphere is formation of the so-called butterfly pitch angle distributions. The first comprehensive survey of such electron pitch angle distributions by OGO5 in the inner magnetosphere and the near-Earth magnetotail was performed by *West et al.* [1973]. In contrast to "standard" pitch angle distributions with an empty loss cone

region (small pitch angles) and maximal fluxes at equatorial pitch angles [e.g., *Bogott and Mozer*, 1971; *West*, 1979; *Gannon et al.*, 2007], the butterfly distribution corresponds to a minimum of fluxes both in the loss cone and near 90° pitch angles. From the earliest observations, the formation of the electron butterfly pitch angle distribution was explained by a combination of the effects of localized injection of charged particles from the magnetotail region and azimuthal energy-dependent drifts [*Luhmann and Vampola*, 1977]. Observations from the ATS-6 spacecraft showed that the decrease of the equatorial magnetic field amplitude on the nightside can be accompanied by formation of electron pitch angle distributions having minima at large pitch angles [*Kaye et al.*, 1978]. Thus, butterfly distributions are associated with the deformed nightside magnetic field configuration. The observational evidence of the formation of butterfly distributions (both for ions and electrons) due to splitting of drift shells in the compressed inner magnetosphere was given by *Wilken et al.* [1986]. Further, the survey of ISEE-1 observations supported the idea of the formation of butterfly pitch angle distributions over a wide energy range (20 keV–2 MeV) due to splitting of drift shells and magnetopause shadowing [*Fritz et al.*, 2003]. Similar results were obtained using the Polar observations of electron pitch angle distributions [*Klida and Fritz*, 2009, 2013]. However, *Gannon et al.* [2007] demonstrated the dominance of electron butterfly distributions in the nightside and higher L shells for energies larger than 500 keV. Thus, electron butterfly distributions can be separated into (1) events when the minimum of equatorial fluxes are observed over a wide energy range (for these cases, the butterfly distributions are also often observed for ions) and (2) events when only high-energy equatorial electrons are absent. In the first case, charged particle losses due to magnetopause shadowing in a compressed magnetosphere seem to be responsible for the formation of butterfly distributions (see discussion of the significant role of inner magnetosphere compression for electron losses in *Kim et al.* [2008], *Ohtani et al.* [2009], and *Turner et al.* [2012]). The second case seems to be more relevant to nightside charged particle nonadiabatic scattering [*Shibahara et al.*, 2010] or adiabatic evolution [*Ebihara et al.*, 2008; *Su et al.*, 2010] in the deformed (stretched) magnetic field configuration. The efficiency of nonadiabatic scattering for formation of butterfly distributions was demonstrated for ions, while for electrons, such a mechanism may work only for very high energies (> 1 MeV).

Strong currents of injected hot ions can significantly deform the magnetic field configuration in the nightside inner magnetosphere [e.g., *Daglis et al.*, 1999]. These currents decrease the equatorial magnetic field and increase the tangential field component. Thus, magnetotail-like configurations with stretched field lines can emerge (see results of empirical models [*Tsyganenko et al.*, 2003; *Sitnov et al.*, 2008; *Kubyshkina et al.*, 2009]). Violation of adiabaticity of charged particle motions in such a magnetic field configuration has been thoroughly investigated both for energetic ions and relativistic electrons [e.g., *Anderson et al.*, 1997; *Delcourt and Belmont*, 1998, and references therein]. The main effect of this motion is due to nonadiabatic jumps of the first adiabatic invariant near the equatorial plane. *Shibahara et al.* [2010] have shown that these jumps can result in the formation of butterfly pitch angle distributions of energetic ions. In this paper, we investigate the same mechanism for relativistic electrons. We combine observations of Van Allen probes and numerical modeling to study electron nonadiabatic scattering in the absence of waves or a compressed magnetopause.

There are two direct applications of our investigation. First, observations of nonadiabatic features in the relativistic electron pitch angle distribution can be used for probing the magnetic field configuration in the nightside inner magnetosphere. This nonadiabatic scattering requires a specific magnetotail-like configuration of magnetic field lines. Very localized in MLT injections of hot magnetotail ions can be responsible for the formation of such configurations, while these injections may not be strong enough to be distinguished in time profiles of the *Dst* index. Thus, direct observations of electron pitch angle distributions can provide a tool for diagnostics of weak injections. Investigation of the role of such injections are important for understanding inner magnetosphere dynamics (e.g., see discussion in *Ukhorskiy et al.* [2011a]).

On the other hand, the inner magnetosphere can be considered as a natural laboratory for investigation on nonadiabatic motion of charged particles in inhomogeneous magnetic field. Well-resolved spacecraft observations of pitch angle distributions give a chance for testing models describing the violation of adiabaticity. These models are important for laboratory devices with trapped plasma (see reviews [*Baldwin*, 1977; *Chirikov*, 1987; *Varma*, 2003] and for astrophysical applications [e.g., *Hall*, 1980]. Moreover, the similar effect of the adiabaticity destruction influences on models of charged particle motion in the reconnection region [e.g., *Egedal and Fasoli*, 2001].

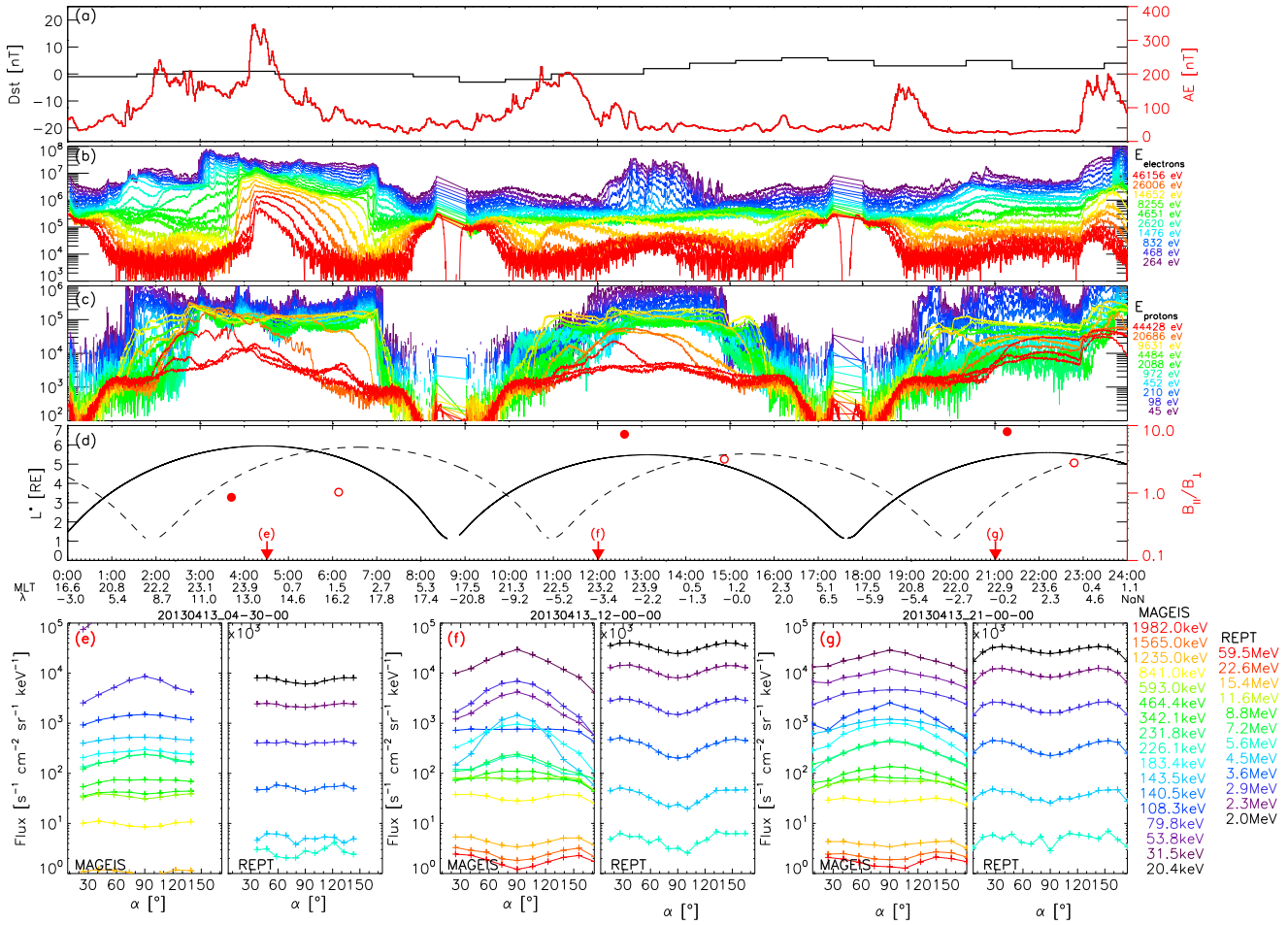

Figure 1. (a) Time profiles of *Dst* and *AE* indices for 1 day of VA Probe observations. (b–g) Time profiles of fluxes of electrons and protons (in cm^{-2} s^{-1} sr−1 keV^{-1}) measured by HOPE onboard VA Probe A, and pitch angle distributions of electrons of different energies (moment of distribution measurements are indicated by red arrows).

2. Observations

The two Van Allen (VA) Probes spacecraft with identical scientific payload were launched in low inclination, highly elliptical orbits with apogees near 5.8 R_E on 30 August 2012 [*Mauk et al.*, 2013]. For this study, we use energetic electron fluxes from the Magnetic Electron Ion Spectrometer (MagEIS) [*Blake et al.*, 2013] and from Relativistic Electron-Proton Telescope (REPT) Instrument [*Baker et al.*, 2013], parts of the Energetic Particle Composition and Thermal Plasma Suite [*Spence et al.*, 2013]; the background and VLF magnetic field and measurements from the Energetic and Magnetic Field Instrument Suite and Integrated Science [*Kletzing et al.*, 2013] magnetometer; VLF electric field measurements from Electric Field and Waves (EFW) instrument [*Wygant et al.*, 2013]. The MagEIS and the REPT instruments provide pitch angle resolved particle fluxes for electrons with energies of 20–4000 keV and of 1.6–18.6 MeV.

In Figure 1 we show the evolution of pitch angle distributions on 13 April 2013 captured by the MagEIS and REPT detectors aboard the VA Probe spacecraft. Figure 1a shows that the geomagnetic activity was rather low with *Dst* ∼ 0 (black curve and the scale at the left), while the *AE* index (red curve and the scale at the right) clearly demonstrates several injections. The most intensive *AE* burst was around 04:00 UT and was accompanied by clear evidence of the electron injection (see the rapid and almost dispersiveless increase of electron fluxes at energies of ∼ 1–40 keV). The ion fluxes do not exhibit a similar increase, thus, the spacecraft was likely located within the electron boundary of injection but eastward relative to the ion boundary [see *Birn et al.*, 1997b, and references therein]. The injection is observed around the midnight sector where pure electron injections without observations of an ion flux increase are not rare (see statistics in *Birn et al.* [1997a]). Observed variations of the electron fluxes show that the injection penetrated to L^* ∼ 5.5. Similar observations

of injection penetration deep into the inner magnetosphere under relatively quiet geomagnetic conditions were recently reported by *Gkioulidou et al.* [2015].

We are mainly interested in electron pitch angle distributions collected at L shell$\sim$ 5–6 in the nightside. The orbital parameters of the VA Probe spacecraft are shown in Figure 1d—the solid line presents L^* of VA Probe A and the dashed line is L^* of VA Probe B (we show both spacecraft orbits to illustrate the deformation of the magnetic field observed by Probes A and B). The magnetic local time (MLT) and magnetic latitude (λ) are indicated at the bottom of Figure 1d for VA Probe A. Intense injections affect the magnetic field topology in the night sector via generation of a nondipole magnetic field component and a decrease of the dipole latitudinal component. To indicate these changes, the values $B_{\|}/B_{\perp}$ (where $B_{\|}$ is the magnetic field component parallel to the local dipole field, and $B_{\perp}$ is the magnetic field component transverse to the local dipole field) at the spacecraft apogees are shown in Figure 1d with red circles (solid for VA Probe A and empty for VA Probe B with the scale at the right). Note that due to the magnetic field reconfiguration, the spacecraft apogees are shifted relative to the maximum value of L^* (compare solid and dashed lines with filled and empty circles, respectively). During intense injection at 4–5 UT, this ratio $B_{\|}/B_{\perp}$ is less than 1 while, in the non-perturbed condition, it is ~10. The pitch angle distributions at the three times indicated by the red arrows are shown in Figures 1c–1e. Before the first injection, all energy channels (from 200 keV up to 4.5 MeV) have pancake pitch angle distributions with a local maximum at $\alpha \sim 90°$ or almost isotropic distributions (for higher energies), see Figure 1e. However, after the injection, the pitch angle distributions are changed significantly (see Figures 1f and 1g). We still observe flux maxima at $\alpha \sim 90°$ for 200–600 keV, while, for larger energies, 3–4.5 MeV, a new type of pitch angle distribution is formed—Figures 1f and 1g. This is the butterfly distribution with a flux maxima at intermediate pitch angles $\alpha \sim 45°$, 135°, and a minimum flux at ~90°. The minimum flux at $\alpha \sim 90°$ is well seen. In contrast to some previous observations [e.g., *Fritz et al.*, 2003; *Klida and Fritz*, 2009, 2013], the butterfly pitch angle distribution is formed only for high energies, while for energies $<$ 1 MeV, the pancake pitch angle distribution is not modified during the entire time interval. A weak minima of fluxes of high-energy equatorial (with $\alpha \sim 90°$) electrons shown in Figure 1e is likely related to the beginning of the formation of the butterfly pitch angle distribution. It is interesting to note that butterfly pitch angle distributions are observed for quite long times (from ~12 up to ~24 UT). Thus, this type of distributions can be considered as a quasi-stationary solution of the pitch angle diffusion equation in this spatial region (note that during the same time interval, similar pitch angle distributions are observed for thermal $\sim$ 1–3 keV ions, see supporting information).

One additional important property of the event shown in Figure 1 is the absence of significant wave emission in the whistler frequency range (not shown, see supporting information). At least, both VA Probes do not record any whistler wave activity during the entire interval of observations. Of course, observations by the VA Probes are rather localized in space at the nightside. However, we observe quasi-stationary electron pitch angle distributions exhibiting the butterfly shape for 12 h interval (i.e., for many periods of azimuthal drifts around the Earth). Thus, there is likely no scattering of electrons on the dayside as well, otherwise the corresponding evolution of pitch angle distributions should be detected. We do not consider an unrealistic situation when the butterfly pitch angle distribution represents the stationary solution of the pitch angle diffusion equation with dominant contribution of particle scattering by waves (to our best knowledge, there is no example of such solutions). For the same reason (stationarity of the pitch angle distribution), we do not consider electron scattering by ULF waves as a possible origin of butterfly distributions (VA Probes also do not detect any significant ULF activity for event under consideration). Moreover, the very low level of the geomagnetic activity with $Dst \sim 0$ indicates that the absence of strong wave emission is rather expected during this time interval. During the 2 day interval (from 12 April to 14 April) the conditions in the solar wind were very quiet: the flow pressure was about 1–2 nPa (without any transients). The solar wind flow velocity decreased from 450 km/s to 380 km/s. Thus, for this event, we do not expect that the magnetopause shadowing effect can play an important role in loses of the equatorial (pitch angle $\alpha \sim 90°$) electrons [e.g., *Shprits et al.*, 2006; *Turner et al.*, 2012].

In Figure 2 we also show pitch angle distributions collected for five other events. In all these events, we deal with quiet conditions (absence of *Dst* variations, absence of whistler wave emissions, absence of transients in the solar wind flow pressure; see supporting information for additional information about these events). Thus, the mechanism responsible for the scattering of high-energy equatorial electrons should correspond to changes of the magnetic field configuration rather than to the wave-particle interaction and/or magnetopause shadowing. Pitch angle distributions shown in Figure 2 exhibit similar flux variations with electron

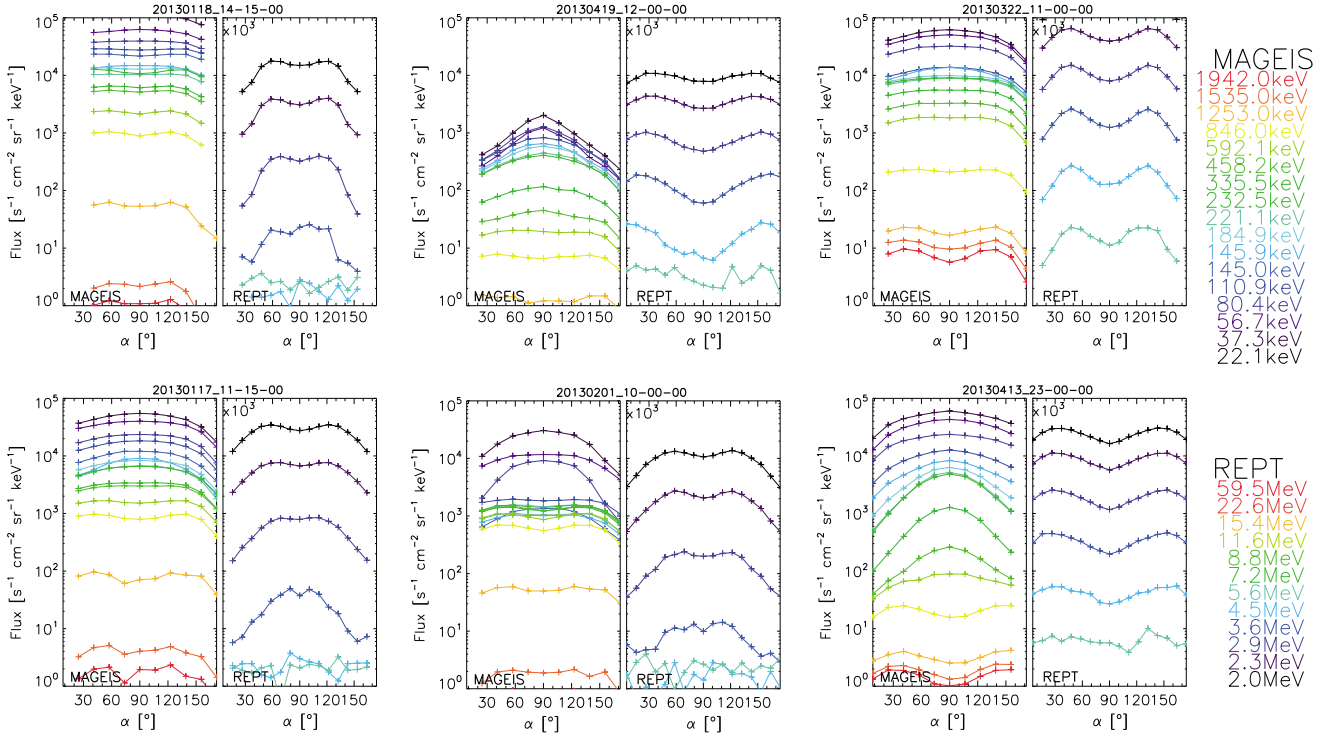

Figure 2. Pitch angle distributions of electrons for six events. The left panels give MAGEIS data, while the right panels show data from the REPT experiment. Energy channels are coded by colors. The last two panels give the event shown in Figure 1, while detailed information including region of observations (MLT and λ) about the other events can be found in the supporting information.

energy. For sub-MeV electrons (energy up to 800 keV) the pitch angle distributions have a distinct maximum at 90°. This is the so-called pancake distribution $\sim\sin^n\alpha$, $n>0$ often observed in the radiation belts [e.g., *Gannon et al.*, 2007]. For electrons with energies ~ 800–1000 keV, we observe flat pitch angle distributions, while minima at $\alpha \sim 0°$ and 180° are also seen. For electrons with energies larger than 1–1.5 MeV the local minimum of fluxes at $\alpha \sim 90°$ is apparent. This minimum is well distinguished in REPT data (see energy channels 2 MeV, 2.3 MeV, and 2.9 MeV). For higher energies (> 3 MeV) the lack of $\alpha \sim 90°$ electrons sometimes disappears. Thus, we can conclude that, in all shown events, the butterfly pitch angle distributions are observed for 1.5–3 MeV electrons.

The time interval of observations of almost stationary (unchanged) pitch angle butterfly distributions shown in Figure 1 is about ~12 h. During this time interval 1–4 MeV electrons turn around the Earth more than 50 times. Thus, we can consider that observed pitch angle distribution as MLT-averaged one. In this case, electrons are not necessarily scattered directly in the region where spacecraft recorded butterfly distributions and, as a result, a local configuration of the magnetic field along VA Probe orbit does not necessarily relate to the magnetic field configuration resulting in electron scattering. For example, relativistic electrons can be scattered within narrow near equatorial region where magnetic field lines are significantly stretched by local currents of hot injected ions. If such region is MLT localized and short living (this seems to be a case for small-scale injections, see *Dubyagin et al.* [2013] and *Gkioulidou et al.* [2014, 2015]), we cannot expect that spacecraft cross the equatorial region exactly in the moment of generation of butterfly distributions. Thus, we have only indirect evidences of the possible role of magnetic field reconfiguration in electron scattering resulting in formation of butterfly pitch angle distributions (e.g., bursts of *AE* index indicate on ion injections, while ratio $B_\parallel/B_\perp \sim 1$ indicates on field line stretching).

The absence of direct measurements of electron scattering within the region with a magnetic field deformation does not allow to specify model parameters directly from the spacecraft observations. However, we can use measurements of the ratio $B_\parallel/B_\perp$ to model the field line stretching. The component $B_\parallel$ of magnetic field corresponds to the local value of the Earth dipole field, while $B_\perp$ represents the magnetic field generated by ion currents. For a weakly disturbed magnetic field configuration we have $B_\parallel/B_\perp \sim 10$ and the dipole

magnetic field dominates (see the second part of the time interval shown in Figure 1). In contrast, just before formation of the butterfly pitch angle distributions, spacecraft detected the significant deformation of the magnetic field: $B_{\|}/B_{\perp} \sim 1$ and the magnetic field amplitude generated by local currents is about the local dipole magnetic field (see the beginning of the time interval shown in Figure 1). In the region of VA Probe observations (magnetic latitude $\lambda < 20°$, L shell ~ 6) the dipole magnetic field is represented equally by B_z and B_x components $B_x/B_z \sim 1.0$ at $\lambda \sim 15°$, while within the near equatorial region $\lambda \sim 5°$ dipole B_z is four times larger than B_x (at the midnight plane). Thus, the 10 time decrease of the ratio $B_{\|}/B_{\perp}$ roughly can be interpreted as a 10 time decrease of the near equatorial B_z magnetic field component (this is the typical effect of ion injection, see *Ganushkina et al.* [2002], *Tsyganenko et al.* [2003], *Le et al.* [2004], *Sitnov et al.* [2008], *Borovsky and Denton* [2010], *Kubyshkina et al.* [2011], and *Dubyagin et al.* [2013]). As a result, at $\lambda \sim 15°$ we should have $B_x/B_z \sim 10$ instead of undisturbed $B_x/B_z \sim 1$. Of course, this very rough estimate cannot be used for the global simulation of electron dynamics in the radiation belts. However, we can use this estimate to model the electron local dynamics (scattering at the vicinity of the equatorial plane) and check if such deformation of the magnetic field is strong enough to provide the electron scattering and formation of the butterfly pitch angle distribution within MLT-localized short time living region. Thus, we use the following logical scheme in our investigation. Due to energy localization and long living of the butterfly pitch angle distributions, these observations likely cannot be explained by mechanisms corresponding to wave-particle interaction and magnetopause shadowing. Moreover, low *Dst*, quiet solar wind, and absence of wave emission observations by VA Probes support this conclusion. On the other side, observations of bursts of *AE* index and $B_{\|}/B_{\perp}$ variations indicate on the possible role of ion injections (and corresponding magnetic field reconfiguration) in electron scattering and formation of butterfly pitch angle distribution. Due to spatial/temporal localization of the region of electron scattering where magnetic field is supposed to be deformed significantly, we do not have a strong observational evidence (e.g., direct observations in this region) of such magnetic field deformation. Thus, we suppose that such deformation really occurs and use test particle simulations to check the corresponding effects on electron scattering. In case, if we reproduce the observed butterfly distribution of relativistic electrons and explain why this distribution is shaped only for high-energy (> 1 MeV) particles, we can use these results as additional confirmation of our scenario of electron scattering.

3. Model of the Electron Scattering

The magnetic moment of charged particles is an adiabatic invariant of motion [*Alfven and Falthammar*, 1963; *Landau and Lifshitz*, 1960], i.e., it is conserved with a certain accuracy depending mainly on the ratio of the time scales of the magnetic field variation and charged particle gyrorotation, and the ratio of scales of magnetic field inhomogeneity and the charged particle Larmor radius. For realistic conditions in the Earth's radiation belts, only the latter ratio is important (in the absence of waves). The disturbed dipole magnetic field in the nightside radiation belts has a local minimum in the equatorial plane. In this region the spatial scale of the magnetic field inhomogeneity (the radius of curvature of the magnetic field lines, R_c) approaches the minimum value. In the same region, a charged particle's Larmor radius ρ has a maximum value due to the minimum of the magnetic field amplitude. Thus, the accuracy of magnetic moment conservation is determined at the equator by the parameter R_c/ρ.

The violation of adiabaticity of the charged particle motion results in a jump of the magnetic moment $\Delta\mu$ (in this paper we use the relativistic adiabatic invariant $\mu = p^2/Bm$ where $p = mc\sqrt{\gamma^2 - 1}$, γ is the gamma factor, m is the rest mass of the charged particle, B is the magnetic field amplitude, see details in *Northrop* [1963] and *Sivukhin* [1965]). In the case of accurate consideration of μ behavior along the trajectory, one can find that the jump $\Delta\mu$ is a sum of many small changes of μ [*Slutskin*, 1964]. However, all these changes are localized around the magnetic field minimum. Thus, to model $\Delta\mu$ we need to approximate correctly the magnetic field configuration in the vicinity of the equator. At this region the B_z components of the magnetic field has a finite value, while the B_x component changes the sign. We consider the charged particles dynamics in the midnight region during a time interval less than 100 of particle bounce periods. For this time interval, MeV electrons can pass the azimuthal distance around ~1–2 MLT hours (see comparison of bounce oscillations and azimuthal drifts of relativistic electrons in *Ukhorskiy and Sitnov* [2013]). Within this region we can neglect the effects of the azimuthal magnetic field component and restrict our consideration to 2-D particle motion in the (x, z) plane. We also consider the effect of the disturbed dipole field with strong currents of hot ions. These currents are localized at the scale $\sim \ell < R_E$ (R_E is the Earth radius) around the equatorial plane [*Le et al.*, 2004; *Dubyagin et al.*, 2013]. There are two main effects of these currents: the significant decrease of the magnetic

field B_z and magnetic field line stretching due to the increase of the B_x component (see, e.g., empirical models [*Sitnov et al.*, 2008; *Kubyshkina et al.*, 2011]). To simulate these two effects one can use the simplified model of the current sheet with the magnetic field $\mathbf{B} = B_0(z/\ell)\mathbf{e}_x + B_z\mathbf{e}_z$, where B_0 is the B_x amplitude. The main difference of this model and the dipole field expanded around the equatorial plane is constant B_z magnetic field component. This simplification comes directly from our assumption about strong localization of a magnetic field perturbation, i.e., the scale ℓ is substantially smaller than the scale of dipole field inhomogeneity $\sim LR_E$. This model is widely used for investigations of charged particle scattering due to nonadiabatic motion [e.g., *Gray and Lee*, 1982; *Birmingham*, 1984; *Delcourt et al.*, 1995]. The Hamiltonian of relativistic electrons with the rest mass m and the charge $-e$ in this magnetic field has the following form:

$$\mathrm{H} = mc^2\sqrt{1 + \frac{p_x^2 + p_z^2}{m^2c^2} + \frac{e^2}{m^2c^4}\left(B_z x - \frac{B_0}{\ell}\frac{1}{2}z^2\right)^2} \tag{1}$$

where (p_x, p_z) are components of the electron momentum (the component p_y is conserved due to the system homogeneity along the y direction; thus, p_y can be removed by a shift of the coordinate origin). Hamiltonian (1) does not depend on time, thus, we can introduce a constant energy H and corresponding gamma factor $\gamma = \mathrm{H}/mc^2 = \mathrm{const}$. We use dimensionless variables: $(p_x, p_z)/\gamma mc \to (p_x, p_z)$, $\mathrm{H}/\gamma mc^2 \to \mathrm{H}$, $(x, z)/l \to (x, z)$ where l is a characteristic spatial scale which is defined below. We also introduce the parameter $\kappa = B_z\ell/B_0 l$. The Hamiltonian (1) takes a form

$$\mathrm{H} = \sqrt{\gamma^{-2} + p_x^2 + p_z^2 + \frac{\Omega_0^2 l^4}{c^2\ell^2\gamma^2}\left(\kappa x - \frac{1}{2}z^2\right)^2} \tag{2}$$

where $\Omega_0 = eB_0/mc$. We chose $l = \sqrt{c\ell\gamma/\Omega_0}$, so that $\Omega_0^2 l^4/c^2\ell^2\gamma^2 = 1$. The new normalized time is $tc/l \to t$. The final form of the Hamiltonian is

$$\mathrm{H} = \sqrt{\gamma^{-2} + p_x^2 + p_z^2 + \left(\kappa x - \frac{1}{2}z^2\right)^2} \tag{3}$$

where $\kappa = (B_z/B_0)\sqrt{\Omega_0\ell/c\gamma}$. For relativistic particles $|\mathbf{p}| \sim mc\gamma$ the parameter κ is equal to $\sqrt{R_c/\rho}$. It is also important to note that the absolute value of normalized Hamiltonian (3) is $\mathrm{H} = 1$. Thus, the Hamiltonian equations for Hamiltonian (3) can be written as

$$\begin{aligned} &\dot{p}_x = -\kappa\left(\kappa x - \frac{1}{2}z^2\right), \quad \dot{p}_z = z\left(\kappa x - \frac{1}{2}z^2\right) \\ &\dot{x} = p_x, \quad \dot{z} = p_z \end{aligned} \tag{4}$$

Due to peculiarities of the used normalization, equation (4) coincide with equations of nonrelativistic charged particle motion in the current sheet [e.g., *Büchner and Zelenyi*, 1989; *Zelenyi et al.*, 2013]. Therefore, we can use results obtained earlier for such a system [*Chen*, 1992; *Delcourt et al.*, 1994, 1996a, 1996b] to describe scattering of relativistic electrons in the radiation belts. Formally speaking, equation (4) can be rewritten in the classical nonrelativistic form with $v_y = (\kappa x - z^2/2)$, $(v_x, v_z) = (p_x, p_z)$:

$$\begin{cases} \dot{v}_x = -\kappa v_y, \quad \dot{v}_z = z v_y \\ \dot{v}_y = \kappa v_x - z v_z \\ \dot{x} = v_x, \quad \dot{z} = v_z, \quad \dot{y} = v_y \end{cases} \tag{5}$$

Such a transformation of a relativistic system (1) to nonrelativistic equation (5) is possible due to conservation of the electron energy in the absence of electric fields.

Let us consider electron dynamics at the geostationary orbit $L = 6.6$ in the case of a strong magnetic field disturbance. According to the empirical models and spacecraft observations [*Ganushkina et al.*, 2002; *Tsyganenko et al.*, 2003; *Le et al.*, 2004; *Sitnov et al.*, 2008; *Borovsky and Denton*, 2010; *Kubyshkina et al.*, 2011; *Dubyagin et al.*, 2013], we take $\ell = R_E$. The same models and the spacecraft observations shown in Figure 1 suggest to use rather small value of the ratio B_z/B_0. The ratio of parallel (i.e., B_z) and transverse (i.e., B_x) magnetic field components is about 1 (in Figure 1) while for dipole field $B_\parallel$ should be much larger than $B_\perp$ along the VA Probe orbit

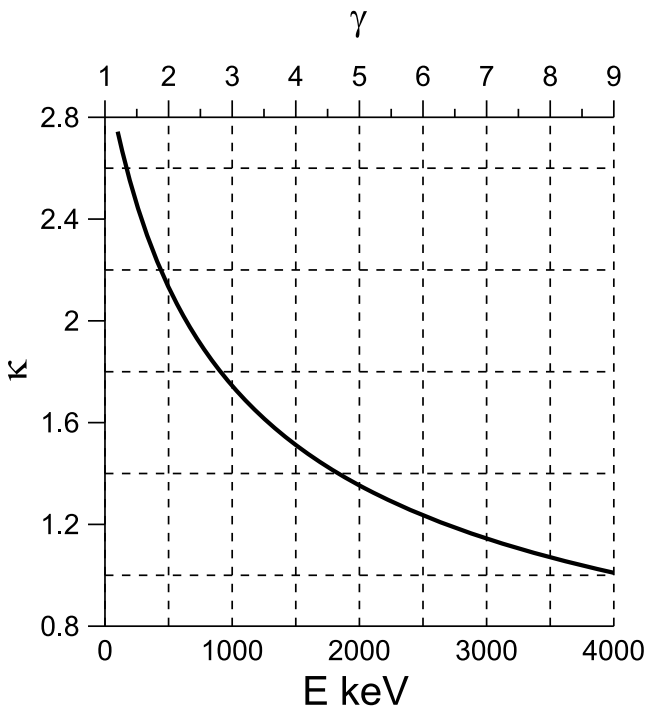

Figure 3. Profile of κ as a function of γ factor and electron energy.

(see the value of the ratio $B_{\parallel}/B_{\perp}$ at the end of time interval shown in Figure 1). Thus, for our modeling, we take $B_z/B_0 \sim 0.15$ (see discussion of this choice in section 2.) In this case, the profile of κ as a function of γ is shown in Figure 3. One can see that 0.5 MeV electrons have $\kappa \approx 2.1$, 2 MeV electrons have $\kappa \approx 1.3$, and 4 MeV electrons have $\kappa \approx 1$. Of course, these values of κ strongly depend on our assumptions of ℓ and B_z/B_0 values.

Several examples of electron trajectories described by this equation (5) are shown in Figure 4. One can see the evolution of the electron equatorial pitch angle α_0 along the trajectory (we calculate this pitch angle at each point using conservation of the total particle energy and the equation for the magnetic moment μ). One can see that for $\kappa = 2.1$ we have a jump $\Delta\alpha_0 \sim 1°$ for the initially almost field-aligned electron. At the distance from the equatorial plane, the magnetic moment (and the equatorial pitch angle α_0) is almost constant. Actually, the magnetic moment μ (and α_0) calculated as a ratio of the perpendicular energy and magnetic field amplitude can oscillate along the trajectory with an amplitude $\sim \kappa^{-2}\mu$ because μ is an approximate integral of motion. However, these oscillations can be removed by introducing the improved adiabatic invariant (see Appendix B for details). This improved adiabatic invariant is equal to μ in certain points along the trajectory. For example, μ calculated at the mirror points conserves with higher accuracy [e.g., *Mozer*, 1966; *Anderson et al.*, 1997]. This property of the magnetic moment is important for understanding the particle trajectory calculated for $\kappa = 2.1$ and a large initial α_0 (see Figure 4). In this case, we deal with oscillations of μ (see oscillations of α_0) along the trajectory, but at the mirror points, values of μ are constant (see insert panel). Thus, even for a large number of particle crossings of the equatorial plane, the equatorial pitch angle does not change, i.e., near-equatorial particles are not scattered in the system with $\kappa = 2.1$. This behavior of $\Delta\alpha_0$ (or $\Delta\mu$) is well described by the semianalytical model developed and tested numerically by *Delcourt et al.* [1994].

The situation is changed for κ=1.3: in this case, we obtain the relatively large jump $\Delta\alpha_0$ even for a near-equatorial electron. This range of κ and α_0 values is already not covered well by the *Delcourt et al.* [1994] model (see discussion in *Shibahara et al.* [2010]). Figure 4 shows that both almost field-aligned and near-equatorial electrons change α_0 substantially during one to a few crossings of the equatorial plane.

Finally, for $\kappa = 1$ we observe almost chaotic behavior of both almost field-aligned and near-equatorial electrons in the vicinity of the equator—the magnetic moment (i.e., α_0) is not an adiabatic invariant anymore [*Northrop*, 1963; *Sivukhin*, 1965] and pitch angle scattering is extremely strong. Particle trajectories in this case resemble Speiser orbits [*Speiser*, 1965, 1967] described by many authors [see *Chen*, 1992; *Zelenyi et al.*, 2013, and references therein].

To demonstrate the effect of electron scattering due to nonadiabaticity of motion, we integrate numerically 10^6 trajectories with an initially uniform distribution of equatorial pitch angles. Each particle trajectory is integrated until it crosses the equatorial plane 40 times. Final distributions are shown in Figure 5 for three values of κ. One can see that for $\kappa = 2.1$ we obtain the distribution without field-aligned particles and with a plateau-like distribution for intermediate to large pitch angles. The same distribution can be obtained analytically using the equations derived by *Delcourt et al.* [1996a, 1996b] (see Appendix A). This semianalytical distribution is shown by the grey curve. Thus, we have electron scattering toward the larger pitch angles with

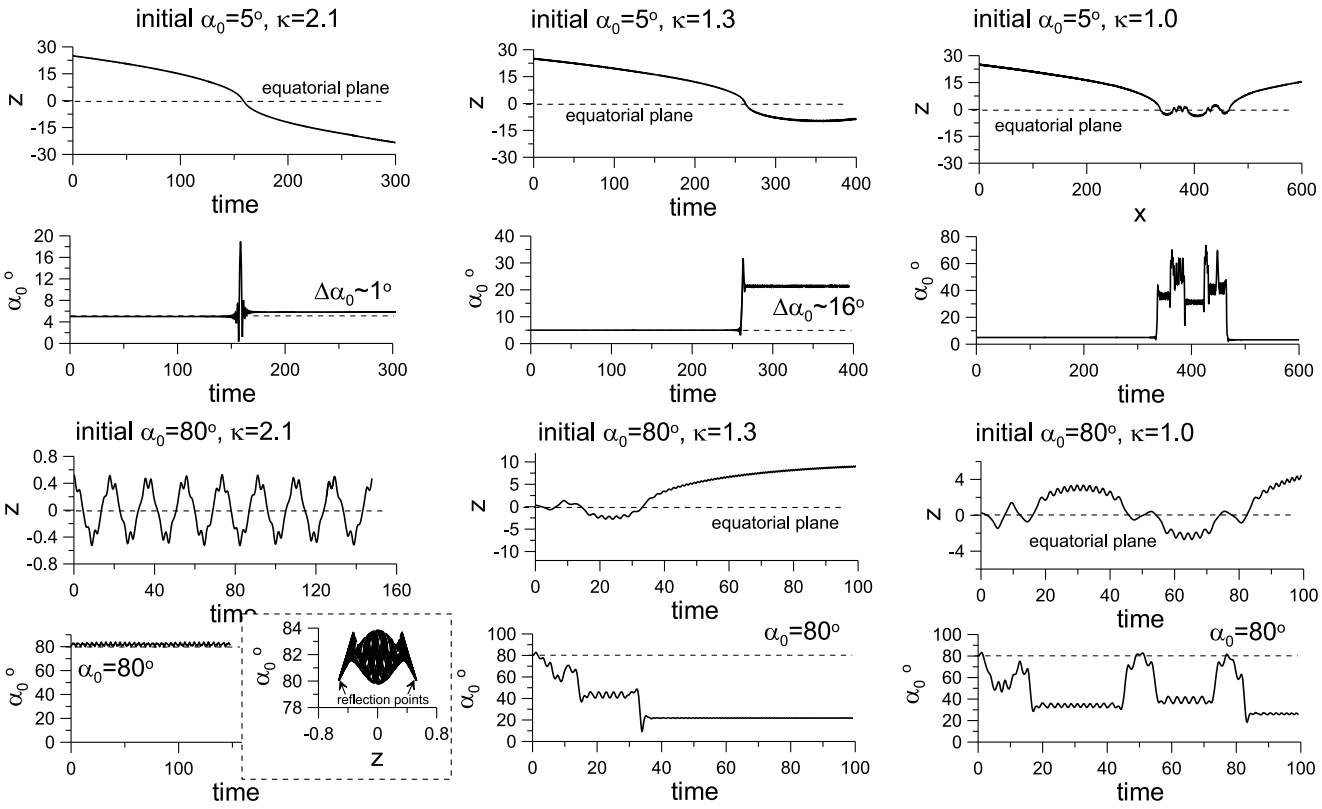

Figure 4. Six trajectories of electrons for $\kappa = 2.1$, $\kappa = 1.3$, $\kappa = 1$, and two values of α_0.

the formation of the classical pancake distribution $\sim \sin^n \alpha_0$, $n > 0$ (see observations by *Gannon et al.* [2007, and references therein]).

For κ=1.3, and κ=1, we obtain distributions with minima at small and large pitch angles. These distributions resemble the butterfly distributions shown in the previous section. The model of *Delcourt et al.* [1996a, 1996b] cannot describe the large pitch angle range of these distributions. The decrease of particle flux at larger pitch angles $\alpha_0 > 60°$ resembles a function $\cos^n \alpha_0$. The dependence of the factor n on κ is estimated in the next section.

4. Electron Pitch Angle Diffusion

To characterize the charged particle scattering in system (5), *Birmingham* [1984] derived the equation for the jump $\Delta\mu$

$$\Delta\mu^* \approx C(\mu^*, \kappa) \cos\vartheta_0 \exp\left(-\kappa^2 F(\mu^*)\right) \tag{6}$$

where $\mu^* = \sin^2 \alpha_0$, the positive function C depends on the initial pitch angle, and κ, ϑ_0 is a gyrophase at the moment of particle crossing the equatorial plane, and the function $F(\alpha_0)$ has the following asymptote for $\alpha_0 \to 90°$ (see Appendix B for details):

$$F(\mu^*) \to -\frac{2}{3} \ln(1 - \mu^*) \tag{7}$$

Thus, for $\mu^* \to 1$ we have

$$\Delta\mu^* \approx C(\mu^*, \kappa)\,(1 - \mu^*)^{2\kappa^2/3} \cos\vartheta_0 \tag{8}$$

While for small μ^*, the asymptote is $\Delta\mu^* \to \sqrt{\mu^*}$. Thus, for the jump of pitch angle $\Delta\alpha_0 = \Delta\mu^* / \sin(2\alpha_0)$ we have

$$\Delta\alpha_0 \approx \cos\vartheta \begin{cases} \text{const}_0, & \alpha_0 \sim 0 \\ \text{const}_1 \cdot \cos^{\frac{2\kappa^2}{3}-1} \alpha_0, & \alpha_0 \sim 90° \end{cases} \tag{9}$$

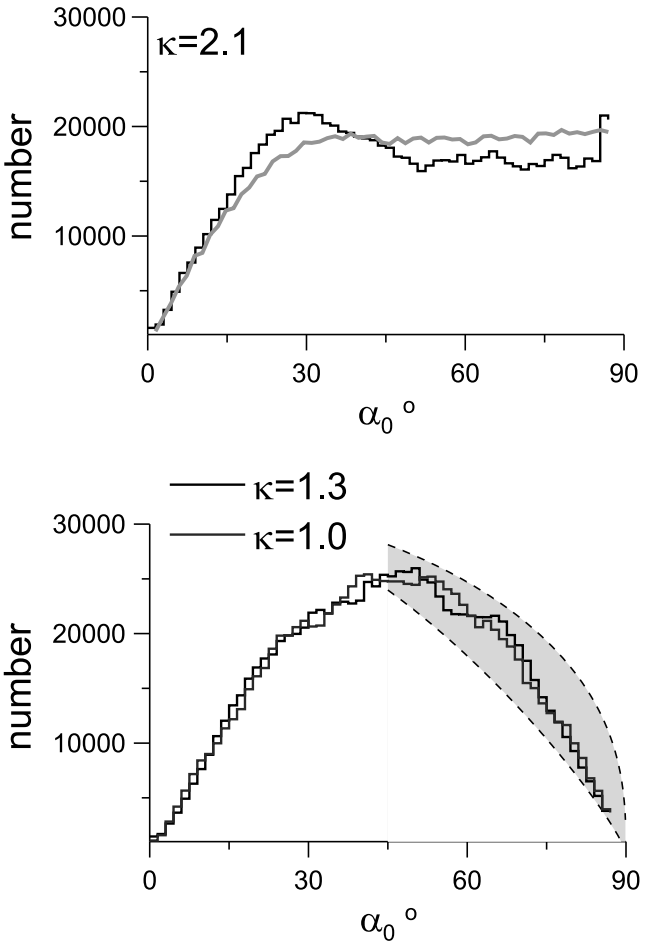

Figure 5. Pitch angle distributions for $\kappa = 2.1$, $\kappa = 1.3$, and $\kappa = 1$. (top) The grey curve shows the semianalytical distribution obtained with a mapping technique (see Appendix A). (bottom) The grey region shows the range between two curves *const* · $\cos^{0.37}\alpha_0$ and const· $\cos^{0.83}\alpha_0$ (see section 4).

Equation (9) shows that for $\kappa > \sqrt{3/2}$ the pitch angle jump becomes small at large pitch angles, while for small κ this jump increases. However, here we should mention that equation (6) was derived for the asymptotic approximation $\kappa \gg 1$ (see Appendix B for details) and a priori should not be valid for $\kappa \sim 1$. Thus, the following conclusion should be taken into account only as an explanation of the numerically obtained results shown in Figure 5.

To estimate the shape of the pitch angle distribution, we use the diffusion equation (the applicability of this equation to the system with nonadiabatic scattering was shown by *Bernstein and Rowlands* [1976], see also *Chirikov* [1987]):

$$\frac{\partial f}{\partial t} = \frac{\partial}{\partial \mu^*}\left(D\frac{\partial f}{\partial \mu^*}\right) \qquad (10)$$

where $f(\mu^*)$ is averaged over bounce oscillations and $D(\mu^*) = \langle(\Delta\mu^*)^2\rangle/\tau(\mu^*)$, τ is the bounce period (the diffusion coefficient is averaged over ϑ_0 values). The stationary solution of equation (10) is

$$f(\mu^*) \sim \int_{\mu^*_{LC}}^{\mu^*} d\tilde{\mu}/D(\tilde{\mu}) \qquad (11)$$

where μ^*_{LC} corresponds to the loss cone angle (i.e., $f(\mu^*_{LC}) = 0$). For small values of μ^*, equation (11) gives $f(\mu^*) \sim \ln(\mu^*/\mu^*_{LC})$ (with $D \sim \mu^*$), while for $\mu^* \to 1$ we have $f(\mu^*) \sim$ const $+ (1-\mu^*)^\eta$ with $\eta = 1 - 4\kappa^2/3$. The distribution $f(\mu^*)$ can be rewritten in terms of pitch angle as $f(\alpha_0) = f(\mu^*)(d\mu^*/d\alpha_0)$:

$$f(\alpha_0) \sim \begin{cases} 2\sin(2\alpha_0)\ln\left(\frac{\sin\alpha_0}{\sin\alpha_{LC}}\right), & \alpha_0 \sim \alpha_{LC} \\ \text{const} + 2\cos^{1+\eta/2}\alpha_0, & \alpha_0 \sim 90° \end{cases} \qquad (12)$$

Equation (12) shows that for $\kappa < 3/2$ (i.e., $1+\eta/2 > 0$), the pitch angle distribution should have a minimum at large pitch angles, because $df/d\alpha_0 \sim -(1+\eta/2) < 0$. Thus, the critical value of κ is about 1.2–1.5: at $\kappa > \sqrt{3/2}$ the pitch angle jumps become small and at $\kappa > 3/2$ the distribution function has a minimum at large pitch angles. The latter criterion is supported by numerical results shown in Figure 5. Of course, all these discussions should be considered carefully because both values of κ are relatively far from the asymptotic range $\kappa \gg 1$ assumed to derive equation (6).

5. Discussion and Conclusions

One of the brightest manifestations of the charged particle nonadiabatic scattering in the nightside inner magnetosphere is observation by high-latitude spacecraft of the so-called boundary of isotropic precipitations [*Imhof et al.*, 1977, 1979; *Sergeev and Tsyganenko*, 1982]. For a given particle energy, this boundary determines that such L shell region that conjugated observations of high-latitude spacecraft demonstrate

almost identical values of fluxes for trapped and precipitating particles. Comparison of models of charged particle scattering and spacecraft observations showed that this boundary is formed by nonadiabatic scattering of charged particles (both protons and electrons) in the equatorial region in the case of significant reconfiguration of the magnetic field (the decrease of the equatorial magnetic field and field line stretching) [*Sergeev et al.*, 1983]. Thus, observations of isotropic boundaries by high-latitude spacecraft can be used for prediction of the magnetic field configuration in the equatorial nightside region [*West et al.*, 1978a, 1978b]. Model results showed that the isotropic boundary can be formed at $\kappa \sim 8$ [*Sergeev et al.*, 1983]. This value of κ is significantly larger than the typical values resulting in scattering of charged particles. However, the isotropic boundary is formed by particles with small pitch angles (only these particles can reach high latitudes), while for these particles the effective κ parameter is smaller than the model κ (see semiempirical model by *Delcourt et al.* [1995, 1996a]). Thus, observation of the isotropic boundary at high latitudes provides an opportunity to estimate the field line radius of curvature in the equatorial plane. In this study we demonstrated the alternative approach for probing the magnetic field configuration with measurements of near-equatorial distributions of high-energy electrons. According to our results, observations of the butterfly pitch angle distributions for certain electron energies should directly tell us about a value of κ. The main advantage of our method corresponds to the local observations of scattered electrons; thus, we can determine a value of κ for a given L shell where butterfly distributions are measured. In contrast, to determine a value of κ from the observations of the isotropic boundaries, one needs to use the magnetic field models to find out the L shell region conjugated to high-latitude measurements. In the case of the significant deformation of the magnetic field configuration, the procedure of such projection is not simple. However, our method cannot provide a global (for different L shells) distribution of κ parameter, while measurements of high-latitude spacecraft allow to calculate κ for different L shells. Thus, both the methods (local observations of the butterfly distributions and high-latitude observations of the isotropic boundary) supplement each other giving more chances to probe a fine structure of the magnetic field configuration in the inner magnetosphere.

The test particle simulations and the analytical estimates presented in section 4 demonstrate that electron scattering in the localized region with the deformed magnetic field can produce the butterfly pitch angle distributions as a stationary solution of the pitch angle diffusion equation. Electrons should cross the equatorial region less than 100 times to shape the almost stationary pitch angle distribution [see also *Shibahara et al.*, 2010]. Thus, the process of formation of butterfly pitch angle distribution requires about 1 min (for >1 MeV electrons at $L \sim 6$, see *Ukhorskiy and Sitnov* [2013]). Here we also can mention the alternative process which can be responsible for electron scattering on time scales of hours (e.g., many azimuthal periods of electron motion). In presence of the deformation of the magnetic field configuration at the dayside, due to action of a solar wind dynamic pressure, relativistic electrons can be scattered by the mechanism involving the bifurcation of drift orbits [see *Shabansky*, 1971]. This mechanism destroys the second adiabatic invariant of electrons providing jumps of equatorial pitch angles (it is especially effective for small pitch angles, see *Ukhorskiy et al.* [2011b]). Particles drifting azimuthally are scattered at the dayside magnetosphere: each pitch angle jump corresponds to one period of azimuthal electron motion; thus, this mechanism is much slower than the destruction of magnetic moment due to electron scattering at nightside (in latter case each jump corresponds to one bounce period). However, as we observed long-living butterfly pitch angle distributions (e.g., Figure 1), the electron scattering due to orbit bifurcation can not be excluded from the consideration. The bifurcation of drift orbits is supported by magnetic field deformation at dayside and, thus, requires relatively significant dynamical pressure of solar wind. For six events shown in Figure 2, a solar wind dynamical pressure varies within following ranges (on 1 day time interval): 17 and 18 January 2013, $P_{sw} \in [1, 15]$ nPa; 1 February 2013, $P_{sw} \in [2, 4]$ nPa; 22 March 2013, $P_{sw} \in [0.5, 1.5]$ nPa, 13 April 2013, $P_{sw} \in [1, 2]$ nPa; and 19 April 2013, $P_{sw} \in [0.7, 1.2]$ nPa. Thus, only for two events (17 January 2013 and 18 January 2013), dynamical pressure is high enough, while for other four events we have rather weak P_{sw} (P_{sw} should be larger than 3 nPa to provide significant scattering of pitch angles within geostationary orbit, see *Ukhorskiy et al.* [2011b, Figure 3]). These data show that the drift orbit bifurcation should be considered in future studies, but this mechanism solely cannot provide electron scattering in all observed events.

Observations of the butterfly distributions by the spacecraft at L shell ~ 6 with conjugated measurements of the magnetic field deformation (e.g., $B_{\|}/B_{\perp} \sim 1$) and particles injections (*AE* bursts) indicate that electron scattering at the deformed magnetic field can be responsible for formation of such distribution. The test particle tracing and analytical estimates confirm that charged particle scattering results in formation of butterfly distributions. Thus, we could notice that nonadiabatic scattering can be important for evolution of

few MeV electron fluxes even if we consider L shell $\sim$ 6 under relatively quiet conditions. Thus, one cannot ignore nonadiabatic effects in modeling the global dynamics of electron fluxes in the radiation belts—these effects potentially can be more important than electron scattering by whistler waves in the nightside [see also *Artemyev et al.*, 2013]. To incorporate nonadiabatic scattering into diffusion models, one should start by calculation of jumps of the adiabatic invariant in the prescribed magnetic field configuration and finish with the construction of diffusion coefficients [e.g., *Bernstein and Rowlands*, 1976; *Rechester and White*, 1980; *Büchner and Zelenyi*, 1989] and numerical testing of final models by means of the trajectory integration or the mapping technique [see, e.g., *Chen et al.*, 1985; *Tagare*, 1986; *Chirikov*, 1987; *Basu and Rowlands*, 1986]. An example of such a closed semianalytical model of nonadiabatic diffusion was proposed by *Young et al.* [2008]. However, two problems should be solved before including this or any similar model in global diffusion codes.

The first problem corresponds to the model peculiarities of electron scattering. The properties of this scattering can significantly vary depending on system parameters. For example, at $\kappa > 3/2$, we do not expect to observe any pitch angle diffusion for equatorial electrons [see *Delcourt et al.*, 1995; *Young et al.*, 2008], while at $\kappa < 3/2$ this diffusion is important (see section 3 and *Shibahara et al.* [2010]). Additionally, in the vicinity of the loss cone (at small pitch angles), the nonadiabatic scattering is nondiffusive (i.e., the averaged jump is not equal to zero and is always positive, see *Delcourt et al.* [1994, 1995]), while analytical estimates give only $\Delta\mu \sim \sin\vartheta_0$ with zero average value for a random uniform distribution of ϑ_0 [*Howard*, 1971; *Cohen et al.*, 1978; *Birmingham*, 1984; *Chirikov*, 1987; *Varma*, 2003]. Moreover, as we discuss in Appendix B, most analytical expressions for $\Delta\mu$ should be tested by numerical calculations because these expressions were derived using not well justified methods. Therefore, more accurate models with thorough numerical testing for wide range of κ are required to correctly simulate the nonadiabatic scattering.

The second problem corresponds to predictions of the magnetic field configuration vitally important for nonadiabatic scattering. The empirical magnetic field models [e.g., *Tsyganenko et al.*, 2003; *Sitnov et al.*, 2008; *Kubyshkina et al.*, 2009] predict the evolution of the magnetic field topology during storm activity when the variation of geomagnetic indexes (*Dst*, K_p, etc.) is well distinguished. However, a change of the magnetic field configuration can potentially be induced by small-scale injections of hot ions from the magnetotail. Such injections (if localized in MLT) may weakly influence the *Dst* index and, as a result, effects of such injections are not included into modern models describing the magnetic field distribution in the inner magnetosphere. Thus, for correct modeling of electron nonadiabatic scattering in the nightside, one needs to collect statistics of modifications of the magnetic field configuration and develop a probabilistic empirical model which can account for small-scale, short-duration events of electron nonadiabatic scattering.

On the other hand, observations of fine-structured pitch angle distributions (e.g., butterfly distributions) in the inner magnetosphere can be applied for testing and improving magnetic field models. The rather common approach corresponds to tracing injected charged particles in model magnetic fields and comparison of result thereby obtained with spacecraft observations. In this case, the global configuration of the model magnetic field can be tested [e.g., *Reeves et al.*, 1991; *Lutsenko et al.*, 2005, 2008]. Thus, a successful reproduction of observed butterfly pitch angle distributions in the framework of test particle modeling should indicate the ability of magnetic field models to simulate the corresponding magnetic field configuration necessary for nonadiabatic electron scattering. Moreover, the recent statistical study of ion butterfly pitch angle distributions in the near-Earth magnetotail [*Wang et al.*, 2013] provides the opportunity for using the same approach to test magnetic field models in this important region. Such testing of empirical magnetic field models is left for future investigations.

Spacecraft observations of pitch angle distributions are significantly influenced by electron propagation along field lines, i.e., the adiabatic electron motion along field lines can change the pitch angle distribution. This is not the case for isotropic distributions [*Whipple et al.*, 1991], but the mapping of anisotropic pitch angle distributions along field lines modifies them in many respects. If we deal with the pancake distribution $\sim \sin^n\alpha_0$ ($n > 0$) then the general shape of this distribution is conserved with electron propagation toward higher latitudes (see Appendix C). However, butterfly pitch angle distributions with $\sim \cos^n\alpha_0$ for equatorial pitch angles changes substantially with latitude and they can almost lose the minimum at perpendicular pitch angles at high latitudes (see Appendix C). Thus, it is important that VA Probes collect butterfly distributions near the equatorial plane where these distributions are not affected significantly by mapping along field lines.

To conclude, in this paper we have shown examples of butterfly pitch angle distributions observed for long time intervals under rather quiet geomagnetic conditions. We have pointed out that observations of butterfly

distributions are accompanied by ion injections (manifested by bursts of *AE* index) and deformation of the dipole magnetic field. We have demonstrated that test particle simulations of electron scattering in deformed magnetic field configuration can reproduce the butterfly distributions as a stationary solution of pitch angle diffusion equation. Based on spacecraft observations and theoretical estimates, we have suggested that electron nonadiabatic scattering can take place even in the rather quiet inner magnetosphere. This scattering may be induced by electron demagnetization in the vicinity of the equatorial plane due to the significant magnetic field deformation in this region by currents of hot injected ions. Thus, observations of butterfly pitch angle distributions of high-energy electrons can be used to probe the magnetic field configuration in the outer radiation belt. We have demonstrated that the theoretical description of nonadiabatic electron scattering should be improved to take into account the effect of significant scattering of equatorial electrons. Our results show that the modulation and shaping of electron pitch angle distributions can result from nonadiabatic effects in the absence of waves and magnetopause shadowing.

Appendix A

Delcourt et al. [1994, 1995] have derived the simple equation describing the charged particle scattering at the magnetic field reversal region. This equation gives the particle pitch angle $\hat{\alpha}_0$ after one passage through the equatorial plane for system (5):

$$\sin^2\hat{\alpha}_0 = \sin^2\alpha_0 + \frac{\cos^4\alpha_0}{g^4(\kappa)} - \frac{2\cos^2\alpha_0\sin\alpha_0}{g^2(\kappa)}\sin\vartheta_0 \tag{A1}$$

where α_0 is an initial pitch angle, ϑ_0 is a gyrophase value at the moment of equator crossing (due to the fast gyrorotation one can assume that ϑ_0 is a quasi-random value with a uniform distribution at $[0, 2\pi]$), while function $g(\kappa)$ is obtained by approximation of numerically calculated trajectories [*Delcourt et al.*, 1996a, 1996b]

$$g(\kappa) = \sqrt{0.65 + \exp\left(\kappa^{1.7} - 1\right)} \tag{A2}$$

Having equation (A1) and assuming ϑ_0 to be a random value, one can construct a simple map $\alpha_0 \rightarrow \hat{\alpha}_0$. There are several peculiarities of this map: (1) all initially field-aligned particles with $\alpha_0 = 0$ already after the first scattering will have the same pitch angle $\hat{\alpha}_0 = \arcsin(g^{-2})$; (2) equatorial particles with $\alpha_0 \approx \pi/2$ are not scattered:

$$\Delta\alpha_0 = \hat{\alpha}_0 - \alpha_0 \approx \frac{\cos^3\alpha_0}{2g^4(\kappa)\sin\alpha_0} - \frac{2\cos\alpha_0}{g^2(\kappa)}\sin\vartheta_0 \tag{A3}$$

and $\Delta\alpha_0 = 0$ for $\alpha_0 = \pi/2$.

Appendix B

In this Appendix B we give a brief overview of theories of the adiabatic invariant conservation and discuss in details the particular expression derived by *Birmingham* [1984]. Historically, the nonadiabatic scattering for particular plasma physical systems was investigated first for magnetic field configurations typical for laboratory mirror traps (see reviews [*Baldwin*, 1977; *Chirikov*, 1987]). However, the general question of accuracy of the adiabatic approximation has an even longer story than applications of this approximation for plasma physics. The exponential estimates of conservation of the adiabatic invariant for charged particle motion in a slowly time varying magnetic field (or a magnetic field slowly depending on coordinates) were obtained more than 50 years ago [*Hertweck and Schlüter*, 1957; *Dykhne*, 1960; *Dykhne and Pokrovskii*, 1961; *Vandervoort*, 1961; *Garrido and Gascón*, 1962], while the rather general approach for derivation of the closed expression for a jump $\Delta\mu$ of the adiabatic invariant was proposed by *Slutskin* [1964].

Let us consider a general Hamiltonian system with a Hamiltonian $\mathrm{H}(r, p, \lambda)$ depending on the slowly changing parameter $\lambda = \lambda(\tau)$ and $\tau = t/\kappa^2$. Conjugated variables (r, p) are changing periodically. One of the examples of such a system is a charged particle motion in the magnetic field slowly changing with time or slowly varying along the particle trajectory. In the 2-D system with the fast gyrorotation and the slow motion along field line, the slow time can be replaced by the coordinate along the field line. It is well known that for such system one can introduce an adiabatic invariant $\mu = (2\pi)^{-1}\oint \mathrm{pdr}$ [*Landau and Lifshitz*, 1960]. The accuracy of conservation of this invariant is defined by the rate of λ variation. The simple transformation of variables $(r, p) \rightarrow (\vartheta, \mu)$ (i.e., guiding center approximation) gives us the following Hamiltonian:

$$\mathrm{H} = \mathrm{H}_0(\mu, \lambda) + \kappa^{-2}\lambda'\mathrm{H}_1(\mu, \vartheta, \lambda) \tag{B1}$$

where $\lambda' = d\lambda/d\tau$ and ϑ is a variable conjugated to μ (i.e., gyrophase). Thus, in the absence of λ variation with time, the invariant μ conserves, while for $\lambda' \neq 0$ we have

$$\dot{\mu} = \frac{\partial \mathrm{H}}{\partial \vartheta} = \kappa^{-2}\lambda' \frac{\partial \mathrm{H}_1}{\partial \vartheta} \tag{B2}$$

Equation (B2) shows that a change of μ is about small parameter κ^{-2}. Moreover, the initial Hamiltonian is periodic relative to the ϑ variation; thus, the variation of μ is also periodic and after averaging over ϑ one can decrease the variation amplitude of μ to $\sim \kappa^{-4}\lambda''$. Such a procedure of averaging can be repeated many times, e.g., *Kulsrud* [1957] showed that a change of μ is about κ^{-2N} where N is a number of possible derivatives of the λ function. If $\lambda(\tau)$ is an analytical function with infinite number of derivatives then the estimate of $\Delta\mu$ is smaller than κ in any degree [*Lenard*, 1959]. In this case, the change $\Delta\mu$ is exponentially small. To derive this estimate one can use the procedure of the infinite number of averagings [e.g., *Nekhoroshev*, 1977].

The modification of the method proposed by *Slutskin* [1964] gives the proof of the exponential accuracy of μ conservation both for Hamiltonian (B1) and for Hamiltonian with slow-fast variables [*Neishtadt*, 2000; *Su*, 2012]:

$$\Delta\mu = O\left(\exp(-a\kappa^2)\right) \tag{B3}$$

where the coefficient a depends only on properties of the λ function. If we can analytically extend the λ function to complex domain Θ: $|\Im\tau| < \mathrm{const}_1 + \mathrm{conts}_2|\Re\tau|$ then $a \geq |Q(\mu,\tau)|$ where level lines of $Q(\mu,\tau)$ are inside the domain Θ and

$$Q = \Im \int_0^\tau \frac{\partial \mathrm{H}_0(\mu,\xi)}{\partial \mu} \mathrm{d}\xi \tag{B4}$$

Equation (B4) shows that the principal factor in estimation of μ conservation is played by singular points of the frequency $\partial \mathrm{H}_0/\partial\mu$ (i.e., gyrofrequency) in the complex plane (there is no singular point of this frequency in the real axis τ for $\lambda(\tau)$ with infinite number of derivatives). For the class of so-called linear systems (i.e., systems where the frequency $\partial \mathrm{H}_0/\partial\mu$ does not depend on μ) the estimate given by equation (B3) can be obtained explicitly by a simple approach [see *Hertweck and Schlüter*, 1957; *Dykhne*, 1960; *Dykhne and Pokrovskii*, 1961; *Vandervoort*, 1961; *Garrido and Gascón*, 1962]. For nonlinear systems with the frequency depending on μ, the estimate given by equation (B3) was derived by *Neishtadt* [1984] [see also *Arnold et al.*, 2006].

Of course, equation (B3) provides only an estimate of accuracy of μ conservation, while equations of $\Delta\mu$ should be derived for any particular system separately (see, e.g., review by *Varma* [2003]). The general approach for $\Delta\mu$ determination consists in integration of equation (B2) along the complex plane with the calculation of the main part of the integral in the singular point τ_0 where the frequency $\partial \mathrm{H}_0/\partial\mu$ equals to zero [*Landau and Lifshitz*, 1960; *Arnold et al.*, 2006]. In case of magnetic field configuration with the cusp region (i.e., X line), *Howard* [1971] derived the expression for $\Delta\mu \sim \exp(-\kappa^2\tilde{F}(\alpha_0))$ for an arbitrary order of singularity $\partial H_0/\partial\mu \sim (\tau - \tau_0)^p$ (here $p > 0$, α_0 is the equatorial pitch angle, i.e., the factor $\tilde{F}$ does not depend on the particle energy). Using the same approach, *Cohen et al.* [1978] obtained expressions for jumps of the magnetic moment in various configurations of magnetic field typical for mirror machines (magnetic traps). Several other configurations of magnetic field were considered in papers by *Chen et al.* [1985], *Tagare* [1986], *Basu and Rowlands* [1986], and *Yavorskij et al.*[2002] (see also reviews by *Chirikov* [1987] and *Varma* [2003]). Some of these expressions for μ were tested with laboratory experiments [*Leffel and Gray*, 1969; *Bora et al.*, 1980; *Notte et al.*, 1993] and numerically [*Rusbridge*, 1977; *Howard*, 1978; *Yavorskij et al.*, 2002].

For system (5) the expression of $\Delta\mu$ was derived by *Birmingham* [1984]:

$$\Delta\mu^* \approx \pi\sqrt{\mu^*}\,(\kappa/2)^{1/4}\cos\vartheta_0 \exp\left(-\kappa^2 F(\mu^*)\right) \tag{B5}$$

where μ^* is the normalized magnetic moment independent on energy ($\mu^* = \sin^2\alpha_0$). The function $F(\mu^*)$ is defined as

$$F(\mu^*) = \int_0^1 \frac{(1-\xi^2)\mathrm{d}\xi}{\sqrt{1-\mu^*\sqrt{1-\xi^2}}} \tag{B6}$$

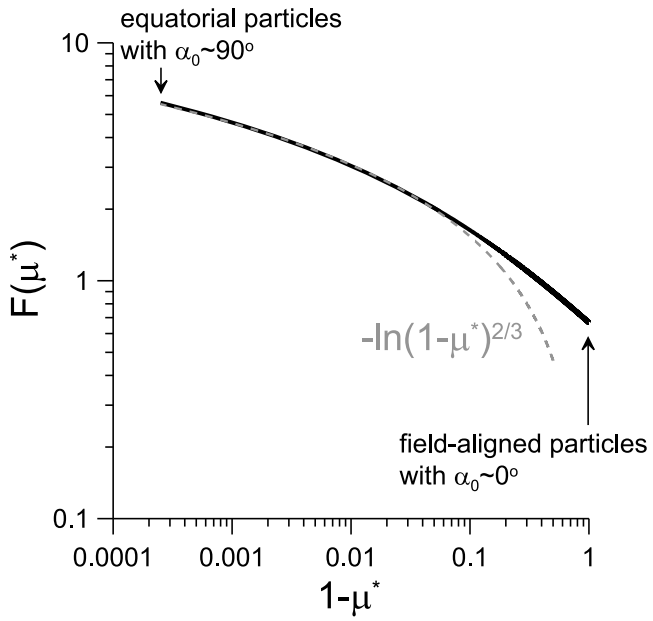

Figure B1. Profile of $F(\mu^*)$ function plotted versus $1\mu^*$.

Figure B1 shows profile of $F(\mu^*)$ and an asymptote for $\mu^* \to 1$ (near-equatorial electrons).

The exponential factor $\sim \kappa^2 F(\mu^*)$ helps us to describe the formation of the butterfly pitch angle distribution. However, here we should notice one important detail about the preexponential coefficient in equation (B5). To derive equation (B5) *Birmingham*[1984] performed the integration in equation (B2) along the unperturbed trajectory, i.e., the conservation of μ was assumed for the integral calculation (the similar approach can be found in many other publications, e.g., *Howard* [1971], *Cohen et al.* [1978], *Chen et al.* [1985], *Tagare* [1986], *Basu and Rowlands* [1986], and *Yavorskij et al.* [2002]). This procedure cannot be fully justified [see *Neishtadt*, 1981]. Adiabatic invariant μ is only an approximate integral of motion, and along the trajectory μ oscillates with an amplitude $\sim \kappa^{-2}$. Thus, an unperturbed trajectory can differ from the real trajectory. This difference potentially can contribute to the final form of an estimation $\Delta\mu$ (see example and discussion of this problem in *Dykhne and Chaplik* [1961]). Thus, one should integrate along the real trajectory including μ variation (in many sense this problem is similar to integration of the dynamical systems with non-Euclidian geometry, see discussion in *Littlejohn* [1988]). One of the possible more rigorous approaches consists in consideration of the jump $\Delta\mu$ as a sum of many small changes (each change corresponds to one period of gyrorotation). In this case, each change is calculated on a small time step when μ is approximately constant, while from step to step the evolution of μ is taken into account [*Slutskin*, 1964]. Therefore, the preexponential factor in equation (B5) can be correct, but this correctness should be tested numerically [see, e.g., *Anderson et al.*, 1997; *Young et al.*, 2002] or with the more accurate analytical approach.

Appendix C

The evolution of the pitch angle distribution along field lines can significantly modify this distribution, especially if it is anisotropic. In this Appendix C we briefly describe the results of mapping of several distributions along field lines. We start with the relativistic Maxwell distribution (i.e., Jüttner distribution, see *Synge* [1957]) $f(\gamma) \sim \gamma^2 \exp(-\gamma/\theta)$ and modify it to include an anisotropy

$$f \sim \gamma^2 \exp\left(-\frac{\gamma}{\theta}\sqrt{1-(1-\gamma^{-2})\chi \sin^2\alpha_0}\right) \tag{C1}$$

where α_0 is the equatorial pitch angle, χ is an anisotropy rate, and $m_e c^2\theta$ is the typical electron energy. For small energies $\gamma \approx 1+(1/2)(v/c)^2$ distribution (C1) transforms to the anisotropic Maxwell distribution. Using the conservation of the magnetic moment and energy, one can recalculate distribution (C1) from the equatorial plane to any point at the field line with a given value of the magnetic field $B = bB_{eq}$ [*Whipple et al.*, 1991]:

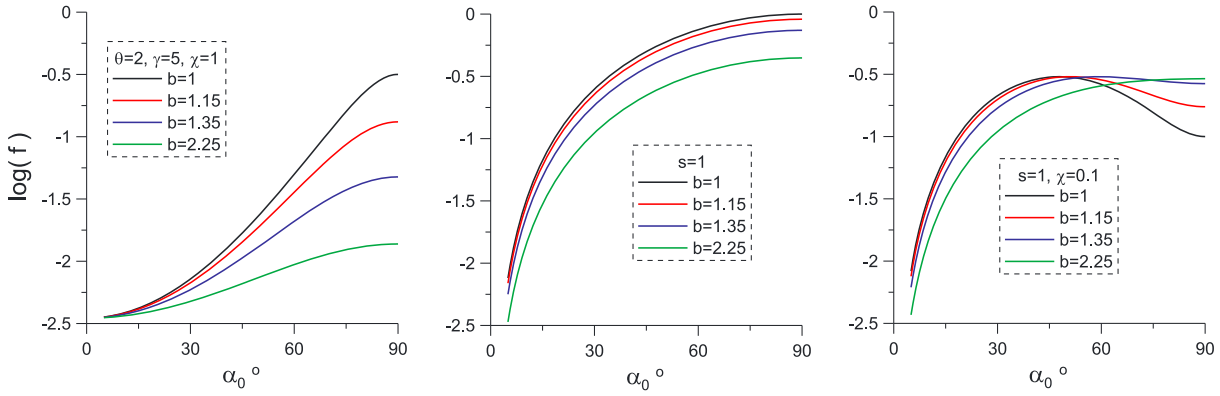

Figure C1. Three examples of evolution of pitch angle distributions with magnetic field relative amplitude *b*.

$$f \sim \gamma^2 \exp\left(-\frac{\gamma}{\theta}\sqrt{1-\chi b^{-1}(1-\gamma^{-2})\sin^2\alpha}\right) \tag{C2}$$

where α is a local value of pitch angle. The similar procedure can be applied to the anisotropic distribution $f \sim \gamma^{-2l}\sin^{2s}\alpha$ (where l and $s \in [0.1, 2]$ are constant parameters) often used for the approximation of spacecraft observations and for analytical estimates [e.g., *Gannon et al.*, 2007; *Summers et al.*, 2009]:

$$f \sim \gamma^{-2l} b^{-s} \sin^{2s}\alpha \tag{C3}$$

We also consider pitch angle distribution with local minimum at the large pitch angles:

$$f \sim \gamma^{-2l}\sin^{2s}\alpha_0(\chi + \cos^2\alpha_0) \tag{C4}$$

with $\chi > 0$. This distribution can be rewritten at some point along field lines as

$$f \sim \gamma^{-2l}\sin^{2s}\alpha\left(\chi + 1 - b^{-1}\sin^2\alpha\right) \tag{C5}$$

Figure C1 shows all three distributions at the equator and calculated for three values of $b = 1.15$, 1.35, and 2.25 (for the dipole field these values correspond to magnetic latitudes 10°, 15°, and 25°). One can see that for distributions (C2) and (C3) the evolution along the field line does not change the shape of α profiles. In contrast, for distribution (C5) the increase of b results in the disappearance of the minimum at large pitch angle.

Acknowledgments
The work was performed under JHU/APL contract 922613 (RBSP-EFW). All data used in this paper can be found at REPT and MagEIS database (http://www.rbsp-ect.lanl.gov/data-pub/) and at RBSP/EFW database (http://www.space.umn.edu/missions/rbspefw-home-university-of-minnesota/).

Michael Balikhin thanks the reviewers for their assistance in evaluating the paper.

References

Åsnes, A., R. W. Friedel, J. Stadsnes, M. Thomsen, N. Østgaard, and T. Cayton (2005), Statistical pitch angle properties of substorm-injected electron clouds and their relation to dawnside energetic electron precipitation, *J. Geophys. Res.*, *110*, A05207, doi:10.1029/2004JA010838.

Alfven, H., and C. G. Falthammar (1963), *Cosmic Electrodynamics*, Clarendon Press, Oxford, U. K.

Anderson, B. J., and K. Takahashi (2000), Pitch angle dispersion of ion injections, *J. Geophys. Res.*, *105*, 18,709–18,727, doi:10.1029/1998JA000332.

Anderson, B. J., R. B. Decker, N. P. Paschalidis, and T. Sarris (1997), Onset of nonadiabatic particle motion in the near-Earth magnetotail, *J. Geophys. Res.*, *102*, 17,553–17,570, doi:10.1029/97JA00798.

Arnold, V. I., V. V. Kozlov, and A. I. Neishtadt (2006), *Mathematical Aspects of Classical and Celestial Mechanics, Dynamical Systems III. Encyclopedia of Mathematical Sciences*, 3rd ed., Springer, New York.

Artemyev, A. V., K. G. Orlova, D. Mourenas, O. V. Agapitov, and V. V. Krasnoselskikh (2013), Electron pitch-angle diffusion: Resonant scattering by waves vs. nonadiabatic effects, *Ann. Geophys.*, *31*, 1485–1490, doi:10.5194/angeo-31-1485-2013.

Baker, D. N., et al. (2013), The Relativistic Electron-Proton Telescope (REPT) instrument on board the Radiation Belt Storm Probes (RBSP) spacecraft: Characterization of Earth's radiation belt high-energy particle populations, *Space Sci. Rev.*, *179*, 337–381, doi:10.1007/s11214-012-9950-9.

Baldwin, D. E. (1977), End-loss processes from mirror machines, *Rev. Modern Phys.*, *49*, 317–339, doi:10.1103/RevModPhys.49.317.

Basu, S., and G. Rowlands (1986), Analytical treatment of charged particle motion in the geomagnetotail, *Planet. Space Sci.*, *34*, 631–637, doi:10.1016/0032-0633(86)90040-1.

Bernstein, I. B., and G. Rowlands (1976), Diffusion in velocity space associated with nonadiabatic changes in the magnetic moment of a charged particle, *Phys. Fluids*, *19*, 1546–1550, doi:10.1063/1.861358.

Birmingham, T. J. (1984), Pitch angle diffusion in the Jovian magnetodisc, *J. Geophys. Res.*, *89*, 2699–2707, doi:10.1029/JA089iA05p02699.
Birn, J., M. F. Thomsen, J. E. Borovsky, G. D. Reeves, D. J. McComas, and R. D. Belian (1997a), Characteristic plasma properties during dispersionless substorm injections at geosynchronous orbit, *J. Geophys. Res.*, *102*, 2309–2324, doi:10.1029/96JA02870.
Birn, J., M. F. Thomsen, J. E. Borovsky, G. D. Reeves, D. J. McComas, R. D. Belian, and M. Hesse (1997b), Substorm ion injections: Geosynchronous observations and test particle orbits in three-dimensional dynamic MHD fields, *J. Geophys. Res.*, *102*, 2325–2342, doi:10.1029/96JA03032.
Blake, J. B., et al. (2013), The Magnetic Electron Ion Spectrometer (MagEIS) instruments aboard the Radiation Belt Storm Probes (RBSP) spacecraft, *Space Sci. Rev.*, *179*, 383–421, doi:10.1007/s11214-013-9991-8.
Bogott, F. H., and F. S. Mozer (1971), Equatorial proton and electron angular distributions in the loss cone and at large angles, *J. Geophys. Res.*, *76*, 6790, doi:10.1029/JA076i028p06790.
Bora, D., P. I. John, Y. C. Saxena, and R. K. Varma (1980), Multiple life times in the nonadiabatic leakage of particles from a magnetic mirror trap, *Plasma Phys.*, *22*, 653–662, doi:10.1088/0032-1028/22/7/003.
Borovsky, J. E., and M. H. Denton (2010), Magnetic field at geosynchronous orbit during high-speed stream-driven storms: Connections to the solar wind, the plasma sheet, and the outer electron radiation belt, *J. Geophys. Res.*, *115*, A08217, doi:10.1029/2009JA015116.
Büchner, J., and L. M. Zelenyi (1989), Regular and chaotic charged particle motion in magnetotaillike field reversals: 1. Basic theory of trapped motion, *J. Geophys. Res.*, *94*, 11,821–11,842, doi:10.1029/JA094iA09p11821.
Chen, G. L., L. W. Owen, D. B. Batchelor, and C. L. Hedrick (1985), Stochastic particle diffusion in velocity space for a bumpy torus, *Phys. Fluids*, *28*, 883–887, doi:10.1063/1.865058.
Chen, J. (1992), Nonlinear dynamics of charged particles in the magnetotail, *J. Geophys. Res.*, *97*, 15,011–15,050, doi:10.1029/92JA00955.
Chen, M. W., J. L. Roeder, J. F. Fennell, L. R. Lyons, and M. Schulz (1998), Simulations of ring current proton pitch angle distributions, *J. Geophys. Res.*, *103*, 165–178, doi:10.1029/97JA02633.
Chirikov, B. V. (1987), *Particle Dynamics in Magnetic Traps*, 1st ed., vol. 13, pp. 1–92, Consultants Bureau, New York.
Cohen, R. H., G. Rowlands, and J. H. Foote (1978), Nonadiabaticity in mirror machines, *Phys. Fluids*, *21*, 627–644, doi:10.1063/1.862271.
Daglis, I. A., R. M. Thorne, W. Baumjohann, and S. Orsini (1999), The terrestrial ring current: Origin, formation, and decay, *Rev. Geophys.*, *37*, 407–438, doi:10.1029/1999RG900009.
Delcourt, D. C., and G. Belmont (1998), Particle dynamics in the near-Earth magnetotail and macroscopic consequences, in *New Perspectives on the Earth's Magnetotail, Geophys. Monogr. Ser.*, vol. 105, edited by A. Nishida, D. N. Baker, and S. W. H. Cowley, p. 193, AGU, Washington D. C.
Delcourt, D. C., R. F. Martin Jr., and F. Alem (1994), A simple model of magnetic moment scattering in a field reversal, *Geophys. Res. Lett.*, *21*, 1543–1546, doi:10.1029/94GL01291.
Delcourt, D. C., J. A. Sauvaud, R. F. Martin, and T. E. Moore (1995), Gyrophase effects in the centrifugal impulse model of particle motion in the magnetotail, *J. Geophys. Res.*, *100*, 17,211–17,220, doi:10.1029/95JA00657.
Delcourt, D. C., G. Belmont, J.-A. Sauvaud, T. E. Moore, and R. F. Martin (1996a), Centrifugally driven phase bunching and related current sheet structure in the near-Earth magnetotail, *J. Geophys. Res.*, *101*, 19,839–19,847, doi:10.1029/96JA01772.
Delcourt, D. C., J.-A. Sauvaud, R. F. Martin, and T. E. Moore (1996b), On the nonadiabatic precipitation of ions from the near-Earth plasma sheet, *J. Geophys. Res.*, *101*, 17,409–17,418, doi:10.1029/96JA01006.
Dubyagin, S., N. Ganushkina, S. Apatenkov, M. Kubyshkina, H. Singer, and M. Liemohn (2013), Geometry of duskside equatorial current during magnetic storm main phase as deduced from magnetospheric and low-altitude observations, *Ann. Geophys.*, *31*, 395–408, doi:10.5194/angeo-31-395-2013.
Dykhne, A. M. (1960), Quantum transitions in the adiabatic approximation, *Soviet J. Exp. Theor. Phys.*, *11*, 411–415.
Dykhne, A. M., and A. V. Chaplik (1961), Variation of the adiabatic invariant for a particle in a magnetic field. II, *Soviet J. Exp. Theor. Phys.*, *13*, 465–467.
Dykhne, A. M., and V. L. Pokrovskii (1961), Change of the adiabatic invariant for a particle in a magnetic field. I, *Soviet J. Exp. Theor. Phys.*, *12*, 264–266.
Ebihara, Y., M.-C. Fok, J. B. Blake, and J. F. Fennell (2008), Magnetic coupling of the ring current and the radiation belt, *J. Geophys. Res.*, *113*, A07221, doi:10.1029/2008JA013267.
Ebihara, Y., M.-C. Fok, T. J. Immel, and P. C. Brandt (2011), Rapid decay of storm time ring current due to pitch angle scattering in curved field line, *J. Geophys. Res.*, *116*, A03218, doi:10.1029/2010JA016000.
Egedal, J., and A. Fasoli (2001), The topology of guiding center orbits in a linear magnetic cusp, *Phys. Plasmas*, *8*, 4042–4052, doi:10.1063/1.1388033.
Fritz, T. A., M. Alothman, J. Bhattacharjya, D. L. Matthews, and J. Chen (2003), Butterfly pitch-angle distributions observed by ISEE-1, *Planet. Space Sci.*, *51*, 205–219, doi:10.1016/S0032-0633(02)00202-7.
Gannon, J. L., X. Li, and D. Heynderickx (2007), Pitch angle distribution analysis of radiation belt electrons based on Combined Release and Radiation Effects Satellite Medium Electrons A data, *J. Geophys. Res.*, *112*, A05212, doi:10.1029/2005JA011565.
Ganushkina, N. Y., T. I. Pulkkinen, M. V. Kubyshkina, H. J. Singer, and C. T. Russell (2002), Modeling the ring current magnetic field during storms, *J. Geophys. Res.*, *107*, 1092, doi:10.1029/2001JA900101.
Garrido, L. M., and F. Gascón (1962), Approximate constancy of adiabatic invariants in plasma physics, *Prog. Theor. Phys.*, *28*, 573–584, doi:10.1143/PTP.28.573.
Gkioulidou, M., A. Y. Ukhorskiy, D. G. Mitchell, T. Sotirelis, B. H. Mauk, and L. J. Lanzerotti (2014), The role of small-scale ion injections in the buildup of Earth's ring current pressure: Van Allen Probes observations of the 17 March 2013 storm, *J. Geophys. Res. Space Physics*, *119*, 7327–7342, doi:10.1002/2014JA020096.
Gkioulidou, M., et al. (2015), Spatial structure and temporal evolution of energetic particle injections in the inner magnetosphere during the 14 July 2013 substorm event, *J. Geophys. Res. Space Physics*, *120*, 1924–1938, doi:10.1002/2014JA020872.
Gray, P. C., and L. C. Lee (1982), Particle pitch angle diffusion due to nonadiabatic effects in the plasma sheet, *J. Geophys. Res.*, *87*, 7445–7452, doi:10.1029/JA087iA09p07445.
Hall, A. N (1980), On the breaking of the first adiabatic invariant in the magnetic fields arising from the mirror instability, *Astron. Astrophys.*, *84*, 40–43.
Hertweck, F., and A. Schlüter (1957), Die "adiabatische Invarianz" des magnetischen Bahnmoments geladener Teilchen, *Z. Naturforsch. Teil A*, *12*, 844–849.
Howard, J. E. (1971), Nonadiabatic particle motion in cusped magnetic fields, *Phys. Fluids*, *14*, 2378–2384, doi:10.1063/1.1693344.
Howard, J. E. (1978), Drift surfaces in linear and axisymmetric magnetic fields, *Plasma Phys.*, *20*, 1185–1197, doi:10.1088/0032-1028/20/11/009.

Imhof, W. L., J. B. Reagan, and E. E. Gaines (1977), Fine-scale spatial structure in the pitch angle distributions of energetic particles near the midnight trapping boundary, *J. Geophys. Res.*, *82*, 5215–5221, doi:10.1029/JA082i032p05215.
Imhof, W. L., J. B. Reagan, and E. E. Gaines (1979), Studies of the sharply defined L dependent energy threshold for isotropy at the midnight trapping boundary, *J. Geophys. Res.*, *84*, 6371–6384, doi:10.1029/JA084iA11p06371.
Kaye, S. M., C. S. Lin, G. K. Parks, and J. R. Winckler (1978), Adiabatic modulation of equatorial pitch angle anisotropy, *J. Geophys. Res.*, *83*, 2675–2682, doi:10.1029/JA083iA06p02675.
Kim, K. C., D.-Y. Lee, H.-J. Kim, L. R. Lyons, E. S. Lee, M. K. Öztürk, and C. R. Choi (2008), Numerical calculations of relativistic electron drift loss effect, *J. Geophys. Res.*, *113*, A09212, doi:10.1029/2007JA013011.
Kletzing, C. A., et al. (2013), The Electric and Magnetic Field Instrument Suite and Integrated Science (EMFISIS) on RBSP, *Space Sci. Rev.*, *179*, 127–181, doi:10.1007/s11214-013-9993-6.
Klida, M. M., and T. A. Fritz (2009), The Earth's magnetopause as a source and sink for equatorial nightside energetic charged particles, *Ann. Geophys.*, *27*, 4305–4316, doi:10.5194/angeo-27-4305-2009.
Klida, M. M., and T. A. Fritz (2013), Characterising electron butterfly pitch angle distributions in the magnetosphere through observations and simulations, *Ann. Geophys.*, *31*, 305–314, doi:10.5194/angeo-31-305-2013.
Kubyshkina, M., V. Sergeev, N. Tsyganenko, V. Angelopoulos, A. Runov, H. Singer, K. H. Glassmeier, H. U. Auster, and W. Baumjohann (2009), Toward adapted time-dependent magnetospheric models: A simple approach based on tuning the standard model, *J. Geophys. Res.*, *114*, A00C21, doi:10.1029/2008JA013547.
Kubyshkina, M., V. Sergeev, N. Tsyganenko, V. Angelopoulos, A. Runov, E. Donovan, H. Singer, U. Auster, and W. Baumjohann (2011), Time-dependent magnetospheric configuration and breakup mapping during a substorm, *J. Geophys. Res.*, *116*, A00I27, doi:10.1029/2010JA015882.
Kulsrud, R. M. (1957), Adiabatic invariant of the harmonic oscillator, *Phys. Rev.*, *106*, 205–207, doi:10.1103/PhysRev.106.205.
Landau, L. D., and E. M. Lifshitz (1960), *Mechanics, Course of Theoretical Physics*, vol. 1, 1st ed., Pergamon Press, Oxford.
Le, G., C. Russell, and K. Takahashi (2004), Morphology of the ring current derived from magnetic field observations, *Ann. Geophys.*, *22*, 1267–1295, doi:10.5194/angeo-22-1267-2004.
Leffel, C. S., Jr., and E. P. Gray (1969), Adiabaticity of charged-particle trajectories in a cusped magnetic field, *Phys. Fluids*, *12*, 1008–1017, doi:10.1063/1.2163661.
Lenard, A. (1959), Adiabatic invariance to all orders, *Ann. Phys.*, *6*, 261–276, doi:10.1016/0003-4916(59)90082-X.
Littlejohn, R. G. (1988), Phase anholonomy in the classical adiabatic motion of charged particles, *Phys. Rev.*, *38*, 6034–6045, doi:10.1103/PhysRevA.38.6034.
Luhmann, J. G., and A. L. Vampola (1977), Effects of localized sources on quiet time plasmasphere electron precipitation, *J. Geophys. Res.*, *82*, 2671–2676, doi:10.1029/JA082i019p02671.
Lutsenko, V. N., I. P. Kirpichev, T. V. Grechko, and D. Delcourt (2005), Source positions of energetic particles responsible for the fine dispersion structures: Numerical simulation results, *Planet. Space Sci.*, *53*, 275–281, doi:10.1016/j.pss.2004.09.053.
Lutsenko, V. N., E. A. Gavrilova, and T. V. Grechko (2008), Statistics of fine dispersion structures events in energetic particle spectra: Their origin and role in the outer magnetosphere, *Ann. Geophys.*, *26*, 2097–2110, doi:10.5194/angeo-26-2097-2008.
Mauk, B. H., N. J. Fox, S. G. Kanekal, R. L. Kessel, D. G. Sibeck, and A. Ukhorskiy (2013), Science objectives and rationale for the radiation belt storm probes mission, *Space Sci. Rev.*, *179*, 3–27, doi:10.1007/s11214-012-9908-y.
Mozer, F. S. (1966), Proton trajectories in the radiation belts, *J. Geophys. Res.*, *71*, 2701–2708, doi:10.1029/JZ071i011p02701.
Neishtadt, A. (1981), On the accuracy of conservation of the adiabatic invariant, *J. Appl. Math. Mech.*, *45*, 58–63, doi:10.1016/0021-8928(81)90010-1.
Neishtadt, A. (1984), The separation of motions in systems with rapidly rotating phase, *J. Appl. Math. Mech.*, *48*, 133–139, doi:10.1016/0021-8928(84)90078-9.
Neishtadt, A. I. (2000), On the accuracy of persistence of adiabatic invariant in single-frequency system, *Regul. Chaotic Dyn.*, *5*, 213–218, doi:10.1070/RD2000v005n02ABEH000143.
Nekhoroshev, N. N. (1977), An exponential estimate of the time of stability of nearly-integrable Hamiltonian systems, *Russ. Math. Surv.*, *32*, 1–65, doi:10.1070/RM1977v032n06ABEH003859.
Northrop, T. G. (1963), *The Adiabatic Motion of Charged Particles*, Interscience Publishers John Wiley, New York-London-Sydney.
Notte, J., J. Fajans, R. Chu, and J. S. Wurtele (1993), Experimental breaking of an adiabatic invariant, *Phys. Rev. Lett.*, *70*, 3900–3903, doi:10.1103/PhysRevLett.70.3900.
Ohtani, S., Y. Miyoshi, H. J. Singer, and J. M. Weygand (2009), On the loss of relativistic electrons at geosynchronous altitude: Its dependence on magnetic configurations and external conditions, *J. Geophys. Res.*, *114*, A01202, doi:10.1029/2008JA013391.
Rechester, A. B., and R. B. White (1980), Calculation of turbulent diffusion for the Chirikov-Taylor model, *Phys. Rev. Lett.*, *44*, 1586–1589, doi:10.1103/PhysRevLett.44.1586.
Reeves, G. D., R. D. Belian, and T. A. Fritz (1991), Numerical tracing of energetic particle drifts in a model magnetosphere, *J. Geophys. Res.*, *96*, 13,997–14,008, doi:10.1029/91JA01161.
Roederer, J. G. (1970), *Dynamics of Geomagnetically Trapped Radiation*, Springer, Berlin.
Rusbridge, M. G. (1977), Non-adiabatic effects in charged particle motion near a neutral line, *Plasma Phys.*, *19*, 1087–1091, doi:10.1088/0032-1028/19/11/009.
Sergeev, V. A., and N. A. Tsyganenko (1982), Energetic particle losses and trapping boundaries as deduced from calculations with a realistic magnetic field model, *Planet. Space Sci.*, *30*, 999–1006, doi:10.1016/0032-0633(82)90149-0.
Sergeev, V. A., E. M. Sazhina, N. A. Tsyganenko, J. A. Lundblad, and F. Soraas (1983), Pitch-angle scattering of energetic protons in the magnetotail current sheet as the dominant source of their isotropic precipitation into the nightside ionosphere, *Planet. Space Sci.*, *31*, 1147–1155, doi:10.1016/0032-0633(83)90103-4.
Shabansky, V. P. (1971), Some processes in the magnetosphere, *Space Sci. Rev.*, *12*, 299–418, doi:10.1007/BF00165511.
Shibahara, K., M. Nosé, T. A. Fritz, and J. Niehof (2010), A new generation mechanism of butterfly pitch angle distributions of energetic ions: Multiple pitch angle scattering in the stretched magnetic field, *J. Geophys. Res.*, *115*, A07229, doi:10.1029/2010JA015281.
Shprits, Y. Y., R. M. Thorne, R. Friedel, G. D. Reeves, J. Fennell, D. N. Baker, and S. G. Kanekal (2006), Outward radial diffusion driven by losses at magnetopause, *J. Geophys. Res.*, *111*, A11214, doi:10.1029/2006JA011657.
Sitnov, M. I., N. A. Tsyganenko, A. Y. Ukhorskiy, and P. C. Brandt (2008), Dynamical data-based modeling of the storm-time geomagnetic field with enhanced spatial resolution, *J. Geophys. Res.*, *113*, A07218, doi:10.1029/2007JA013003.
Sivukhin, D. V. (1965), *Motion of Charged Particles in Electromagnetic Fields in the Drift Approximation*, vol. 1, pp. 1–104, Consultants Bureau, New York.
Slutskin, A. A. (1964), Motion of a one-dimensional nonlinear oscillator under adiabatic conditions, *Soviet J. Exp. Theor. Phys.*, *18*, 676–682.

Speiser, T. W. (1965), Particle trajectories in model current sheets: 1. Analytical solutions, *J. Geophys. Res.*, *70*, 4219–4226, doi:10.1029/JZ070i017p04219.
Speiser, T. W. (1967), Particle trajectories in model current sheets: 2. Applications to auroras using a geomagnetic tail model, *J. Geophys. Res.*, *72*, 3919–3932, doi:10.1029/JZ072i015p03919.
Spence, H. E., et al. (2013), Science goals and overview of the Radiation Belt Storm Probes (RBSP) Energetic Particle, Composition, and Thermal Plasma (ECT) suite on NASA's Van Allen Probes mission, *Space Sci. Rev.*, *179*, 311–336, doi:10.1007/s11214-013-0007-5.
Su, T. (2012), On the accuracy of conservation of adiabatic invariants in slow-fast Hamiltonian systems, *Regular Chaotic Dyn.*, *17*, 54–62, doi:10.1134/S1560354712010054.
Su, Z., F. Xiao, H. Zheng, and S. Wang (2010), Combined radial diffusion and adiabatic transport of radiation belt electrons with arbitrary pitch angles, *J. Geophys. Res.*, *115*, A10249, doi:10.1029/2010JA015903.
Summers, D., R. Tang, and R. M. Thorne (2009), Limit on stably trapped particle fluxes in planetary magnetospheres, *J. Geophys. Res.*, *114*, A10210, doi:10.1029/2009JA014428.
Synge, J. L. (1957), *The Relativistic Gas*, North-Holland Pub. Co., Amsterdam.
Tagare, S. G. (1986), Motion of charged particles in an axisymmetric magnetic mirror, *Phys. Rev. A*, *34*, 1587–1590, doi:10.1103/PhysRevA.34.1587.
Tsyganenko, N. A., H. J. Singer, and J. C. Kasper (2003), Storm-time distortion of the inner magnetosphere: How severe can it get?, *J. Geophys. Res.*, *108*, 1209, doi:10.1029/2002JA009808.
Turner, D. L., Y. Shprits, M. Hartinger, and V. Angelopoulos (2012), Explaining sudden losses of outer radiation belt electrons during geomagnetic storms, *Nat. Phys.*, *8*, 208–212, doi:10.1038/nphys2185.
Ukhorskiy, A. Y., and M. I. Sitnov (2013), Dynamics of radiation belt particles, *Space Sci. Rev.*, *179*, 545–578, doi:10.1007/s11214-012-9938-5.
Ukhorskiy, A. Y., B. H. Mauk, N. J. Fox, D. G. Sibeck, and J. M. Grebowsky (2011a), Radiation belt storm probes: Resolving fundamental physics with practical consequences, *J. Atmos. Sol. Terr. Phys.*, *73*, 1417–1424, doi:10.1016/j.jastp.2010.12.005.
Ukhorskiy, A. Y., M. I. Sitnov, R. M. Millan, and B. T. Kress (2011b), The role of drift orbit bifurcations in energization and loss of electrons in the outer radiation belt, *J. Geophys. Res.*, *116*, A09208, doi:10.1029/2011JA016623.
Vandervoort, P. O. (1961), The nonconstancy of the adiabatic invariants, *Ann. Phys.*, *12*, 436–443, doi:10.1016/0003-4916(61)90070-7.
Varma, R. K. (2003), Classical and macroquantum dynamics of charged particles in a magnetic field, *Phys. Rep.*, *378*, 301–434, doi:10.1016/S0370-1573(03)00005-X.
Wang, C.-P., S. G. Zaharia, L. R. Lyons, and V. Angelopoulos (2013), Spatial distributions of ion pitch angle anisotropy in the near-Earth magnetosphere and tail plasma sheet, *J. Geophys. Res. Space Physics*, *118*, 244–255, doi:10.1029/2012JA018275.
West, H. I., Jr. (1979), The signatures of the various regions of the outer magnetosphere in the pitch angle distributions of energetic particles, in *Quantitative Modeling of Magnetospheric Processes, Geophys. Monogr. Ser.*, vol. 21, pp. 150–179, AGU, Washington, D. C., doi:10.1029/GM021p0150.
West, H. I., Jr., R. M. Buck, and J. R. Walton (1973), Electron pitch angle distributions throughout the magnetosphere as observed on Ogo 5, *J. Geophys. Res.*, *78*, 1064–1081, doi:10.1029/JA078i007p01064.
West, H. I., R. M. Buck, and M. G. Kivelson (1978a), On the configuration of the magnetotail near midnight during quiet and weakly disturbed periods: Magnetic field modeling, *J. Geophys. Res.*, *83*, 3819–3831, doi:10.1029/JA083iA08p03819.
West, H. I., Jr., R. M. Buck, and M. G. Kivelson (1978b), On the configuration of the magnetotail near midnight during quiet and weakly disturbed periods: State of the magnetosphere, *J. Geophys. Res.*, *83*, 3805–3817, doi:10.1029/JA083iA08p03805.
Whipple, E., R. Puetter, and M. Rosenberg (1991), A two-dimensional, time-dependent, near-Earth magnetotail, *Adv. Space Res.*, *11*, 133–142, doi:10.1016/0273-1177(91)90024-E.
Wilken, B., D. N. Baker, P. R. Higbie, T. A. Fritz, and W. P. Olson (1986), Magnetospheric configuration and energetic particle effects associated with a SSC - A case study of the CDAW 6 event on March 22, 1979, *J. Geophys. Res.*, *91*, 1459–1473, doi:10.1029/JA091iA02p01459.
Wygant, J. R., et al. (2013), The electric field and waves instruments on the radiation belt storm probes mission, *Space Sci. Rev.*, *179*, 183–220, doi:10.1007/s11214-013-0013-7.
Yavorskij, V. A., D. Darrow, V. Y. Goloborod'ko, S. N. Reznik, U. Holzmueller-Steinacker, N. Gorelenkov, and K. Schoepf (2002), Fast ion non-adiabaticity in spherical tokamaks, *Nucl. Fusion*, *42*, 1210–1215, doi:10.1088/0029-5515/42/10/306.
Young, S. L., R. E. Denton, B. J. Anderson, and M. K. Hudson (2002), *Empirical Model for μ Scattering Caused by Field Line Curvature in a Realistic Magnetosphere*, 1069, vol. 107.
Young, S. L., R. E. Denton, B. J. Anderson, and M. K. Hudson (2008), Magnetic field line curvature induced pitch angle diffusion in the inner magnetosphere, *J. Geophys. Res.*, *113*, A03210, doi:10.1029/2006JA012133.
Zelenyi, L. M., A. I. Neishtadt, A. V. Artemyev, D. L. Vainchtein, and H. V. Malova (2013), Quasiadiabatic dynamics of charged particles in a space plasma, *Physics Uspekhi*, *56*, 347, doi:10.3367/UFNe.0183.201304b.0365.